https://doi.org/10.1016/j.tws.2023.111079

Local buckling behaviour of high strength steel and hybrid I-sections under axial compression: Numerical modelling and design

Shuxian, Chen[a], Jun-zhi, Liu[b,1,*], Tak-Ming Chan[a]

a Department of Civil and Environmental Engineering, The Hong Kong Polytechnic University, Hong Kong, China

b School of National Safety and Emergency Management, Beijing Normal University, China

(1. Formerly, Department of Civil and Environmental Engineering, The Hong Kong Polytechnic University, Hong Kong, China.)

Abstract: This paper presents a numerical investigation on the local buckling behaviour of high strength steel (HSS) and hybrid I-sections under axial compression, which hasn't been comprehensively discussed in previous literature. Three sectional steel combinations, featuring different web strength grades (Q690, Q460, and Q355) and using HSS Q690 flange plates, were studied. Through the validated numerical method, parametric studies on the effect of web strength grade, boundary condition and plate slenderness were carried out. The design specifications in European, Australian, and American codes were evaluated using the results of 243 numerical models and collated test data. In addition, the continuous strength method (CSM), direct strength method (DSM), and Kato's method, which can account for element interaction were extended to design for the local buckling behaviour of HSS and hybrid I-sections subjected to axial compression. Assessment results showed that ANSI/AISC 360-16 provides more accurate results than Eurocode 3 and AS 4100. Statistical and reliability results demonstrated the satisfactory reliability level of the proposed design expressions for CSM, DSM, and Kato's design methods. This paper provides insight into the local buckling behaviour and mechanism behind plate interaction of hybrid I-sections.

Key words: local buckling behaviour; high strength steel; hybrid I-section; design method; axial compression

1. Introduction

In steel frame construction, I- or H-profiles are widely used as compression members due to their ease of connection. High strength steel (HSS) members, which offer a high strength-to-weight ratio, are increasingly favoured, particularly for high-rise structures. The behaviour of HSS I- and H-section compression members has thus garnered attention among researchers seeking to promote the use of lighter and stronger structures.

Because of their higher yield strength, HSS I-/H-sections feature thinner-wall plates, which means

that the local buckling behaviour plays a crucial role in the design of HSS I-/H-shaped compression members. Despite that HSS structural components were applied as early as the 1960s (Miki et al., 2002; Pocock, 2006), it was the thriving developments in the steel manufacturing industry in the 1990s that renewed interest in the behaviour of HSS members (Miki et al., 2002). Since then, studies on the local buckling behaviour of welded HSS I-sections in compression have emerged. Rasmussen and Hancock (1992) suggested that the same yield slenderness limits in specifications for normal strength steel (NSS) can be applied to the HSS plates based on the experimental test results of BISALLO Y 80 (nominal yield strength $f_{y,nom}$= 690 MPa) box, cruciform, and I-section stub columns. Shi et al. (2014; 2015) investigated the local buckling of Q460 ($f_{y,nom}$= 460 MPa) and 960 MPa ($f_{y,nom}$= 960 MPa) I-sections under axial compression through experiments and numerical methods, and found that both European and American codes (EN 1993-1-12:2007, 2007; ANSI/AISC 360-10, 2010) provide over-conservative predictions for I-sections members with slender flanges. After that, Shi et al. (2016) carried out extensive parametric studies on the local buckling behaviour of welded stub columns made from steel materials with nominal yield strengths of 235 MPa, 460 MPa, 690 MPa, and 960 MPa respectively. Based on the research work, modified formulas that take steel strength into consideration were proposed. Sun et al. (2019) conducted experimental tests and finite element (FE) analysis of S690 welded I-section stub columns under axial compression. It was concluded that the design rules in Eurocode 3 (EN 1993-1-12:2007, 2007), ANSI/AISC 360-16 (2016), and AS 4100-1998 (2016) generally provide safe and accurate predictions. Cao et al. (2020) studied the local buckling behaviour of 800 MPa HSS welded I-section stub columns, and proposed slenderness magnifying coefficients for both the flange and web plate to consider the flange-web interactive effect. Li et al. (2019) and Su et al. (2021) examined S960 ultra-high strength steel (UHSS) I-section stub columns under axial compression, and the results revealed that the AISC specification (ANSI/AISC 360-16, 2016) gave the most satisfactory results, in terms of plate slenderness limits and design strength.

Hybrid design of steel I-sections, which utilise different strength steels for plate elements, have gained attention alongside the evolution of HSS materials. Hybrid I-sections with higher strength flange plates than the web typically serve as flexural members, as the web plate of I-sections makes a comparatively small contribution under bending. There is fairly limited published literature on the local buckling behaviour of hybrid I-sections in compression, with the earliest studies dating back to the 1960s. Through test analysis, NagarajaRao et al. (1965; 1969; 1972) found that partial or whole inelastic web local buckling might occur at the ultimate load due to the lower strength of the web. After that, Yun et al. (2021) reported the stub column test results on two hybrid I-sections with S690 flanges and S355 webs, as well as four HSS S690 I-sections. It was observed that when a plateau is featured in the axial load-end shortening curve of HSS I-sections, hybrid counterparts exhibit a strain

hardening region after reaching the yield load due to the development of plasticity in the lower strength web. More recently, a companion paper by the authors (2023a) reported that the ultimate cross-section resistance of hybrid I-sections under axial compression is influenced by the web strength grade, even for specimens with the elastic local buckling web. The above research findings indicate that the lower strength of the web under axial compression can significantly affect the local buckling behaviour of hybrid I-sections. However, there is still a lack of comprehensive analysis on this topic.

Furthermore, evidence has suggested that the interactive effect of flange and web plates (i.e., element interaction) exists in I-/H-sections in compression (Bedair, 2009; Bai and Wadee, 2015; Shi et al., 2016; Cao et al., 2020). American and Japanese specifications for the design of steel structures (ANSI/AISC 360-16, 2016; AIJ LSD, 2010) have also taken this element interaction into account, whilst most codified design methods, such as EN 1993-1-1:2005 (2005) and AS 4100 (AS, 2020) follow "individual plate rule".

This study aims to investigate the local buckling behaviour of HSS and hybrid I-sections under axial compression. I-sections comprising Q690 ($f_{y,nom}$= 690 MPa) flanges and webs made of different strength grades ($f_{y,nom}$ = 690, 460, 355 MPa) were compared. Based upon the validated numerical models, an extensive parametric study was conducted to explore the effect of web strength, boundary condition, and plate slenderness on the local buckling behaviour of HSS and hybrid I-section stub columns. A total of 243 established models, as well as the collated test data were adopted to evaluate the applicability of codified design methods. Furthermore, newly developed design approaches were extended to account for flange-web interaction in the local buckling behaviour of HSS and hybrid I-sections subjected to compression.

2. Finite element modelling

2.1 Finite element models

Commercial finite element analysis (FEA) software suite-ABAQUS 2019 was utilised to perform numerical analysis for I-sections in compression. Geometric dimensions of I-section are shown in **Fig. 1**. In this figure, b_f and t_f are the width and thickness of flange; H and h_w denote the section height and the clear distance between flanges; t_w is the thickness of web plate; h_f represent the fillet weld size.

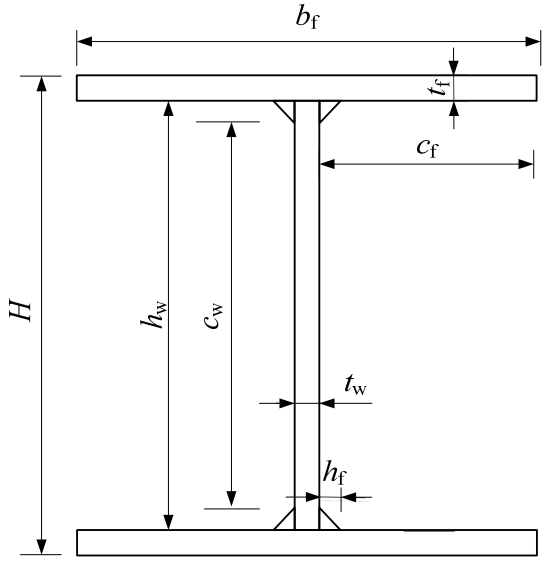

Fig. 1. Notation of I-section

Fixed-ended boundary condition was selected for parametric studies to investigate the local buckling behaviour of I-section stub columns. As illustrated in **Fig. 2**, except for the longitudinal displacement, all the other translational and rotational degrees of freedom are restrained for both ends of I-sections. A 4-node shell element with finite membrane strains-S4R was adopted with the element size equal to the plate thickness for balancing the simulation accuracy and computational cost after sensitivity analysis (Chen et al., 2023a). Based on the multi-linear stress-strain constitutive model, the true stress-strain relation converted from the measured engineering curves of tensile coupon test results (Chen et al., 2023b) were imported as material parameters of FE models. The basic material characteristics of steel plates are presented in **Table 1**, where "Q690-F" and "Q690-W" are characterised by 690 MPa nominal yield strength ($f_{y,nom}$= 690 MPa). In this study, "Q690-F" was selected to be material characteristics of flange plate, and "Q690-W", "Q460-W" ($f_{y,nom}$= 460 MPa) and "Q355-W" ($f_{y,nom}$= 355 MPa) were used for web plates. In **Table 1**, E is the elastic modulus; ε_y, ε_{sh} and ε_u denote the yield strain, strain at the onset of strain hardening and ultimate strain; f_y and f_u mean the yield strength and ultimate strength of steel materials.

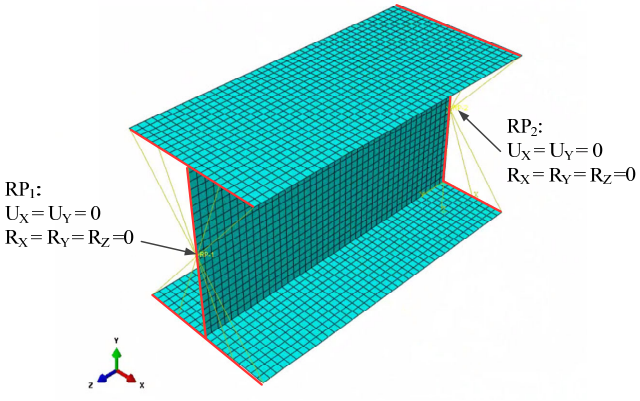

Fig. 2. Boundary condition of fixed-ended I-section models

Table 1. Basic material characteristics of steel plates used in finite element analysis

Steel	E (GPa)	ε_y (%)	ε_{sh} (%)	ε_u (%)	f_y (MPa)	f_u (MPa)
Q690-F	217.4	0.377	3.42	6.75	819.5	848.4
Q690-W	216.1	0.365	2.46	6.86	788.9	834.5
Q460-W	215.8	0.241	1.13	13.6	520.9	663.5
Q355-W	213.2	0.179	1.24	17.2	382.0	553.3

Initial imperfections, including the welding-induced residual stress and local geometrical imperfection, are considered for numerical simulation. Experimental investigation on the membrane residual stresses of HSS and hybrid I-sections has been reported by authors (Chen et al., 2023b). It was observed that the residual stress distribution is marginally influenced by steel strength grade, and a new residual stress distribution model applicable to the investigated I-sections was proposed. The membrane residual stress distribution model used in numerical analysis is illustrated in **Fig. 3**, the detailed information can be found in Chen et al. (2023b). The residual stress is introduced by inputting the initial stress to predefined fields of the model.

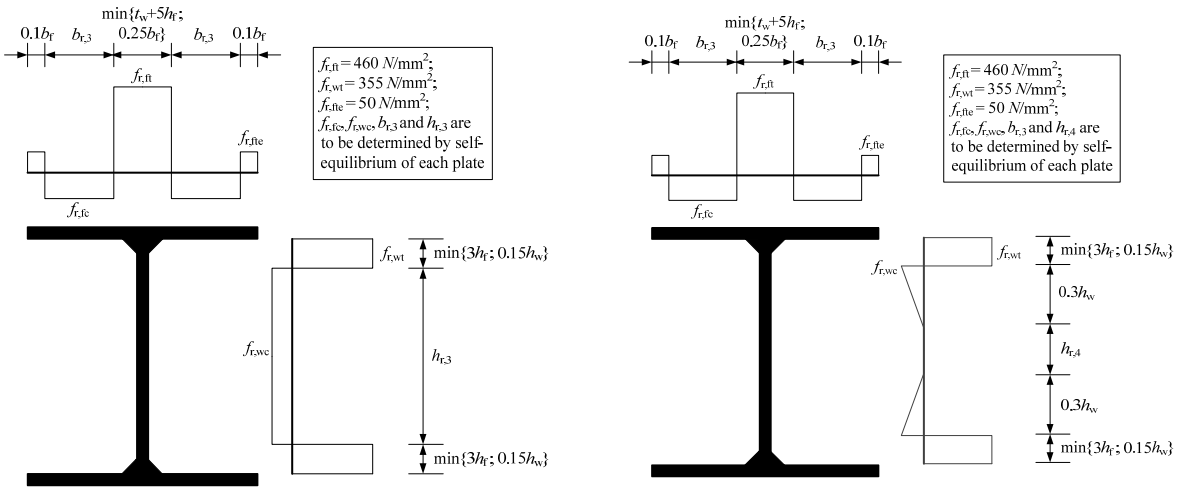

(a) for I-sections with $h_w \leqslant 210$ mm (b) for I-sections with $h_w \geqslant 210$ mm

Fig. 3. Residual stress distribution model used in numerical analysis

Besides, the initial local imperfection of I-sections has been measured in Chen et al. (2023a). The measurement results showed that average measured local imperfection magnitude of outstand flange-1/49 was close to the one (1/50) recommended in EN 1993-1-5:2006 (2006) for finite element modelling, while the average magnitude (1/817) for the internal web plate was less than that (1/200) in Eurocode 3. The local geometric imperfection of the I-section was introduced by importing the first eigenvalue buckling mode obtained from linear perturbation analysis under loading conditions (Chen et al., 2023a).

The newly developed residual stress predictive model for I-sections and the local imperfection magnitudes recommended by Eurocode 3 were applied to numerical models for parametric analysis after validation. The fillet welds at web-flange junction of welded I-sections were ignored in the modelling, because of the limited influence (Tse, et al., 2021; Zhu, et al., 2023; Yun et al., 2023).

2.2 Validation

Compression test results reported in authors' experimental studies for fixed-ended I-section stub columns (Chen et al., 2023a) was chosen to validate the effectiveness of FE method in this study. All the test series for I-sections with 230 mm, 330 mm and 440 section heights, labelled as "H230", "H350" and "H440" in **Table 2**, were replicated. The nominal width and thickness for the flange plates of I-sections were 110 mm and 10 mm, and the nominal web thickness was 6 mm. Three web strength grades-$f_{y,nom}$= 690, 460, 355 MPa were considered for each section dimension. The nomenclature of test specimens follows the sequence of section height and web strength grade. For "H230" series, member lengths of 1.2h_w and 2.2h_w (denoted by L1 and L2 in **Table 2**) were adopted

to study the effect of stub column length on the compression behaviour of I-sections. A detailed discussion on the length effect has been presented in Chen et al. (2023a).

Table 2. Comparison of ultimate test loads and numerical results for I-section stub columns

Series	Specimen	$N_{u,test}$ (kN)	Measured imperfection		e_{EC3}	
			$N_{u,FE}$ (kN)	$N_{u,FE}/N_{u,test}$	$N_{u,FE}$ (kN)	$N_{u,FE}/N_{u,test}$
H230	H230-690W-L1	2674	2625	0.98	2604	0.97
	H230-690W-L2	2641	2564	0.97	2527	0.96
	H230-460W-L1	2458	2394	0.97	2373	0.97
	H230-460W-L2	2378	2347	0.99	2307	0.97
	H230-355W-L1	2369	2271	0.96	2250	0.95
	H230-355W-L2	2302	2252	0.98	2213	0.96
H350	H350-690W	2802	2743	0.98	2734	0.98
	H350-460W	2445	2427	0.99	2417	0.99
	H350-355W	2371	2273	0.96	2256	0.95
H440	H440-690W	2887	2824	0.98	2810	0.97
	H440-460W	2422	2421	1.00	2422	1.00
	H440-355W	2363	2269	0.96	2260	0.96
	Mean			0.98		0.97
	CoV			0.013		0.015

In **Table 2**, ultimate test loads $N_{u,test}$ of specimens were compared with FE models with measured imperfection as well as those with the suggested values in Eurocode 3 (e_{EC3}). Seen from this table, local imperfection magnitude has a negligible impact on the ultimate loads of I-sections failed by local buckling in compression, as the mean ratios of numerical ultimate loads $N_{u,FE}$ to $N_{u,test}$ are 0.98 and 0.97, with the corresponding Coefficient of Variation (CoV) of 0.013 and 0.015 for models with measured imperfection and e_{EC3}.

The failure modes of test and FE results for "H230-690W-L2" are set out in **Fig. 4**. It can be observed that the numerical model can capture the local buckling behaviour of specimen accurately. In addition, taking "H230-460-L2", "H350-460" and "H440-460" as representatives, axial load N versus end shortening δ_u curves of test and FE models with e_{EC3} are depicted in **Fig. 5**. It can be seen from these figures that the simulation results of axial load-end shortening response from FE models with e_{EC3} are consistent with the test curves, thus proving the effectiveness of the adopted FE method.

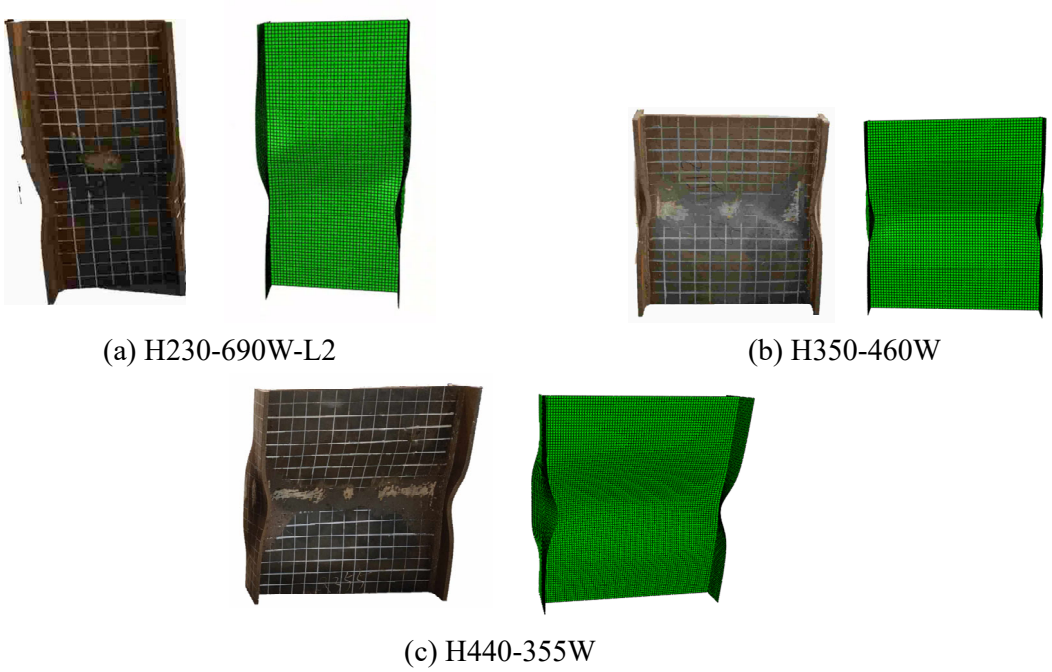

Fig. 4. Comparison of failure modes of selected I-section stub columns between test and finite element model

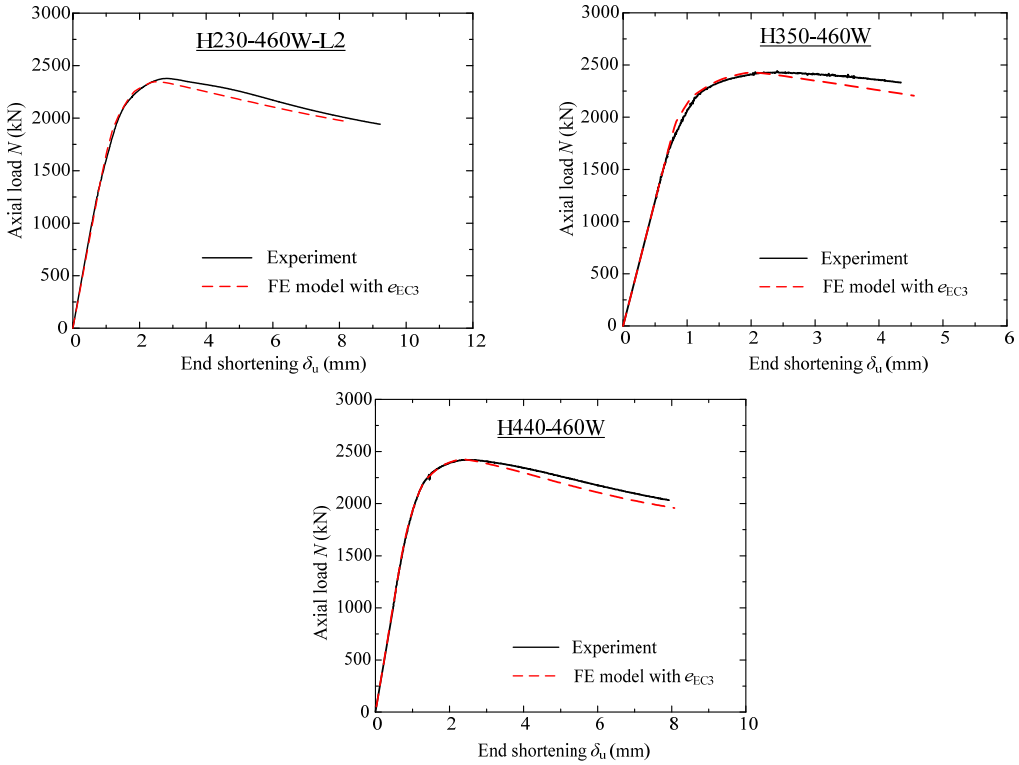

Fig. 5. Comparison of axial load-end shortening curves between test and finite element models with the recommended local imperfection magnitude in Eurocode 3-e_{EC3}

3. Parametric study

To identify the local buckling behaviour of I-sections under axial compression, FE models with geometrical characteristics presented in **Table 3** were established. The thicknesses of flange and web plates were selected to be equal to 10 mm and 6 mm. Referring to the ratios for local buckling of flange (c_f/t_f) and web plates (c_w/t_w) of universal columns in BS EN 10365 (2017), the ranges of flange width b_f and web height h_w were 50~420 mm and 30~420 mm, respectively, and the ratio of flange local buckling parameter-c_f/t_f to web local buckling parameter-c_w/t_w was selected to between 1.5 and 5 as reasonable column section dimensions. c_f represents the distance from flange outstand edge to weld, and c_w means the distance between welds along the web plate, as shown in **Fig. 1**. For each cross-section dimension, three sectional steel combinations were considered, all of which were made of Q690 flange, but with different web strength grade steels-Q690, Q460 and Q355, expressed as "HO-690", "HY-690+460" and "HY-690+355" in this study. Three times the widest overhanging width of plates $L=3b_o$ was selected to be the length of I-section stub columns to eliminate the effect from the end restraint of loaded edges (Timensoko and Gere,1961). I-sections failed with the occurrence of overall buckling takes place were excluded in the parametric study.

Table 3. Geometric characteristics of I-sections for parametric study (mm)

t_f=10; t_w=6; (c_f/t_f)/(c_w/t_w) =1.5~5;
b_f = 50, 60, 70, 75, 80, 90, 100, 115, 130, 145, 160, 180, 200, 240, 280, 360, 420;
h_w = 30, 40, 50, 60, 70, 80, 90, 100, 110, 120, 130, 140, 150, 180, 210, 240, 270, 300, 330, 360, 420;

In the subsequent subsections, representative I-sections are selected to investigate the effect of web strength grade, boundary condition of loaded edges and plate slenderness on the local buckling behaviour of HSS and hybrid I-sections under axial compression. Geometric characteristics of the selected representative I-sections are tabulated in **Table 4**. In this table, $\sigma_{cr,w,SS}$ and $\sigma_{cr,f,SS}$ represent the critical elastic buckling stress of web and flange plates with simply-supported unloaded edges according to theory of elastic stability (Timoshenko & Gere, 1961), which can be obtained using Equation (1). In this equation, $\sigma_{cr,SS}$ denotes the elastic critical buckling stress of the plate with simply-supported unloaded edges; k_{SS} is the buckling coefficient under the corresponding boundary condition, i.e., k_{SS} = 4 for the internal web plate, k_{SS} = 0.43 for the outstand flange plate for the studied I-sections in compression; b_p and t denote the width and thickness of the plate, and E and v are the material's Young's modulus and Poisson's ratio, respectively.

$$\sigma_{\mathrm{cr,SS}} = k_{\mathrm{SS}} \frac{\pi^2 E}{12\left(1-\nu^2\right)}\left(\frac{t}{b_{\mathrm{p}}}\right)^2 \quad (1)$$

In **Table 4**, Φ in is the ratio of $\sigma_{\mathrm{cr,f,SS}}$ to $\sigma_{\mathrm{cr,w,SS}}$, taken as a reference benchmark to determine the critical plate of I-sections (flange or web) (Gardner et al., 2019; Fieber et al., 2019). As given by Equation (2), when Φ is greater than unity, the elastic local buckling stress and half-wavelength of the whole I-section is governed by the web, and $\Phi<1$ indicates that flange plate controls the elastic local buckling behaviour of I-section.

$$\Phi = \frac{\sigma_{\mathrm{cr,f,SS}}}{\sigma_{\mathrm{cr,w,SS}}} = \begin{cases} >1 & \text{web is crtical} \\ <1 & \text{flange is crtical} \end{cases} \quad (2)$$

Table 4. Geometric characteristics of representative I-sections

Specimen	b_{f}	h_{w}	$\sigma_{\mathrm{cr,f,SS}}$	$\sigma_{\mathrm{cr,w,SS}}$	Φ	Critical Plate
			$N_{\mathrm{u}}>N_{\mathrm{y}}$			
B80-H70	80	50	6132	11245	0.55	flange
B75-H80	75	60	7053	7809	0.90	flange
B60-H80	60	60	11515	7809	1.47	web
			$N_{\mathrm{u}}\approx N_{\mathrm{y}}$			
B90-H90	90	70	4759	5737	0.83	flange
B90-H120	90	100	4759	2811	1.69	web
B75-H120	75	100	7053	2811	2.51	web
			$N_{\mathrm{u}}<N_{\mathrm{y}}$			
B160-H130	160	110	1416	2323	0.61	flange
B160-H260	160	240	1416	488	2.90	web
B420-H260	420	240	196	488	0.40	flange
B420-H440	420	420	196	159	1.23	web

These I-sections are categorised into three types in terms of the stress distribution and local buckling behaviour of plate elements: (1) the plates experience a distinct strain hardening stage ($N_{\mathrm{u}}>N_{\mathrm{y}}$); (2) the plates are in the yield plateau stage ($N_{\mathrm{u}}\approx N_{\mathrm{y}}$); (3) the plates undergo the elastic local buckling ($N_{\mathrm{u}}<N_{\mathrm{y}}$). N_{u} and N_{y} are the ultimate axial load and yield load of I-section stub columns. The calculation of N_{y} can be expressed by Equation (3), where f_{yf} and A_{f} represent the yield strength and gross area of flange plates, and f_{yw} and A_{w} are the yield strength and area of web.

$$\begin{cases} N_y = f_{yf} \times A_f + f_{yw} \times A_w \\ A_f = 2 \times b_f \times t_f \\ A_w = h_w \times t_w \end{cases} \quad (3)$$

3.1 Effect of web strength grade

3.1.1 I-sections with $N_u > N_y$

Among I-sections with $N_u > N_y$, "B80-H70" models own comparatively stocky web plates. With Φ = 0.55, this I-section dimension is characterised with the critical flange plate. **Fig. 6** displays the stress contours for the web of "B80-H70" models at the ultimate load N_u, where the region in red reaches the ultimate stress of materials. It is apparent from this figure that "B80-H70" model with Q690 web-"HO-690" presents a broader red zone than hybrid I-sections-"HY-690+460" and "HY-690+355" models. The reason behind it is that the ultimate strain ε_u of "Q690-W" is much less than that of "Q460-W" and "Q355-W", as presented in **Table 1**.

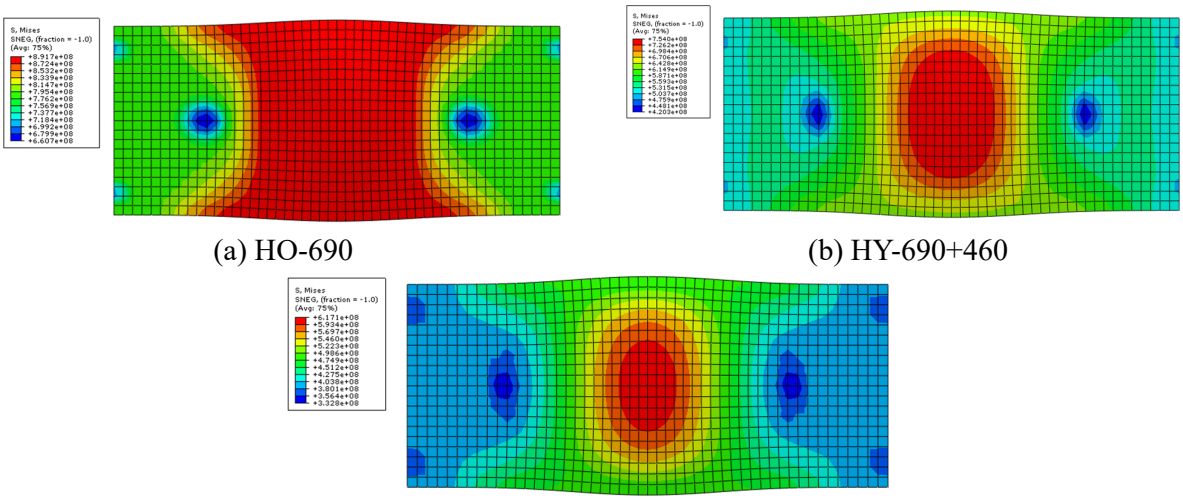

(a) HO-690 (b) HY-690+460

(c) HY-690+355

Fig. 6. Stress contours of the web for "B80-H70" models at the ultimate load

Fig. 7(a) and **(b)** shows the normalised axial load N/N_y against lateral deflection of the flange δ_f and web δ_w of "B80-H70" models. Seen from these figures, no remarkable difference was observed among N/N_y-δ_f curves, but an abrupt turn was detected in N/N_y – δ_w curves of "HY-690+460" and "HY-690+355" curves. It might be explained by the fact that the local deformation of the flange causes the opposite movement of web plate to its local buckling. It can be illustrated by the displacement contour of web plate at the ultimate load in **Fig. 7(c)**, with "HY690+355" as an example, that opposite displacement occurs between the edges and centre of the web plate.

(a) Normalised axial load-flange lateral deflection curves

(b) Normalised axial load-web lateral deflection curves

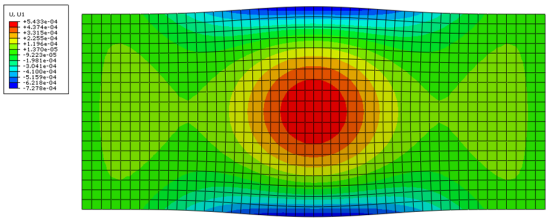

(c) Displacement contour of web plate for "HY690+355" model at the ultimate load

Fig. 7. Deformation characteristics of "B80-H70" I-section models

In addition, classified into I-sections with $N_u > N_y$, "B75-H80" and "B60-H80" models, with Φ = 0.90 and 1.47, are flange-critical and web-critical I-sections, respectively. Seen from **Fig. 8(a)**, the web lateral deflection of flange-critical "B75-H80" I-sections is still affected by the flange, revealed by the unsmoothed curves of I-sections. Comparatively, "B60-H80" models, of which the web plate is critical, similar N/N_y-δ_w curves are presented for I-sections with different webs, as provided in **Fig. 8(b)**.

(a) "B75-H80" models

(b) "B60-H80" models

Fig. 8. Normalised axial load against web lateral deflection of the selected I-sections with $N_u > N_y$

3.1.2 I-sections with $N_u \approx N_y$

In **Table 4**, "B90-H90", "B90-H120" and "B75-H120" are chosen as representatives with $N_u \approx N_y$. Among them, "B90-H90" I-section is flange-critical, whilst "B90-H120" and "B75-H120" are web-critical I-sections. Normalised axial load N/N_y-end shortening δ_u curves of these models with different web are compared in **Fig. 9**. For "B90-H90" models, no apparent distinction was observed for HSS and hybrid I-sections; For "B90-H120" models, a yield plateau was found for hybrid I-sections with Q460 and Q355 webs, but not for HSS homogeneous Q690 section; For "B75-H120" models, the curves of "HY-690+460" and "HY-690+355" I-sections exhibit an obvious strain hardening stage, which was not detected in the "HO-690" curve. These findings are consistent with the experimental observation of Yun et al. (2021) described in introduction.

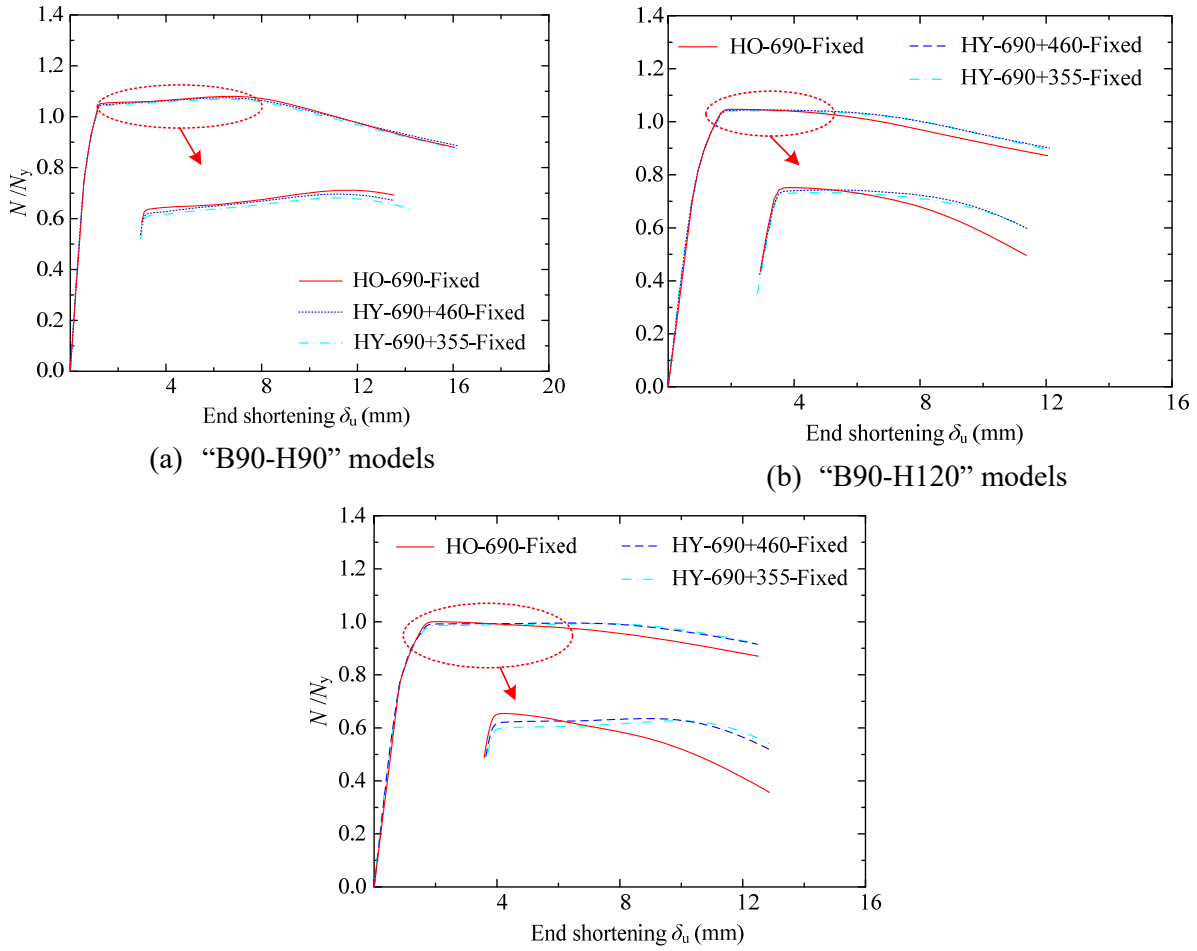

(a) "B90-H90" models

(b) "B90-H120" models

(c) "B75-H120" models

Fig. 9. Normalised axial load-end shortening curves of I-sections with $N_u \approx N_y$

Taking I-sections with Q690 web as an instance, **Fig. 10** provides the stress contour of "B90-H120"

and "B90-H90" models at the ultimate load N_u. It could be observed that though the flange geometry is identical, the distinctive stress state and distribution are found between these two I-sections with different web height: for "B90-H90" model with Q690 web, a portion of flange has reached the ultimate true stress-906MPa and presents an obvious local deformation; for "B90-H120" model with Q690 web, the majority of flange zone is still in the yield plateau. This phenomenon reveals the interactive effect between flange and web plates, which can also be demonstrated by the comparison of N/N_y-δ_u curves between "B90-H120" and "B75-H120" I-sections in **Fig. 9**.

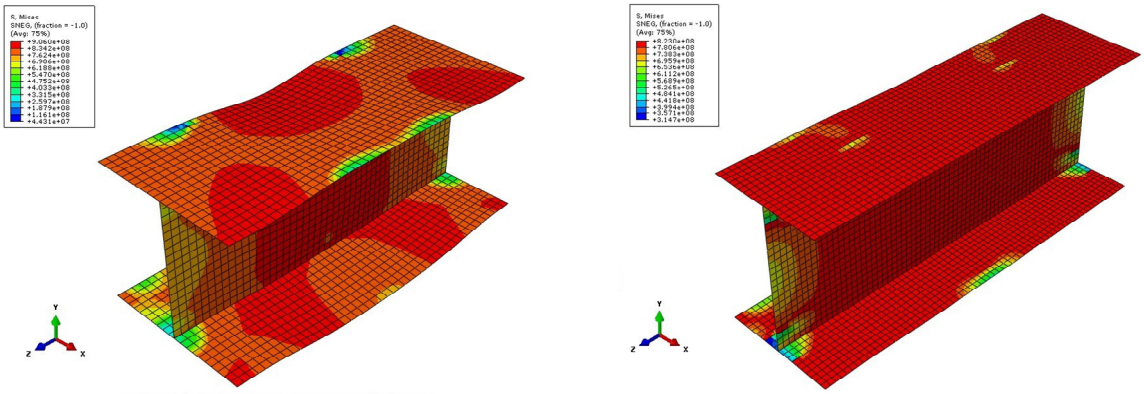

(a) "B90-H90" model with Q690 web (b) "B90-H120" model with Q690 web

Fig. 10. Stress contours of the selected I-sections with $N_u \approx N_y$ at the ultimate load

3.1.3 I-sections with $N_u < N_y$

Among the four representative I-sections of which N_u is less than N_y in **Table 4**, "B160-H130"and "B420-H260" models is the ones with flange element as the critical plate, when the web element is more critical than the flange for "B160-H260" and "B420-H440" models.

Based on Bleich's empirical expression of web critical elastic buckling stress $\sigma_{cr,w}$ in I-sections (Bleich, 1952), which has been proved by test data (Chen et al., 2023a), the value of $\sigma_{cr,w}$ of "B420-H440" is 229 MPa, revealing that it is elastic local buckling that occurs in the critical web plate element. For "B420-H260" models, $\sigma_{cr,w}$ is 850 MPa, but its elastic local buckling stress of the whole cross-section based on Gardner's prediction approach (Gardner et al., 2019) is 274 MPa, which indicates the critical flange plate of "B420-H260" I-sections experience an early elastic local buckling-i.e., less than 274 MPa.

Fig. 11(a) shows N-δ_f curves of flange-critical "B420-H260" I-sections, where the coincident pre-buckling paths but diverse post-buckling curves were presented among models with different webs. A similar phenomenon was discovered in the pre-buckling and post-buckling stages in N-δ_w of the web-critical "B420-H440 models (**Fig. 11(b)**).

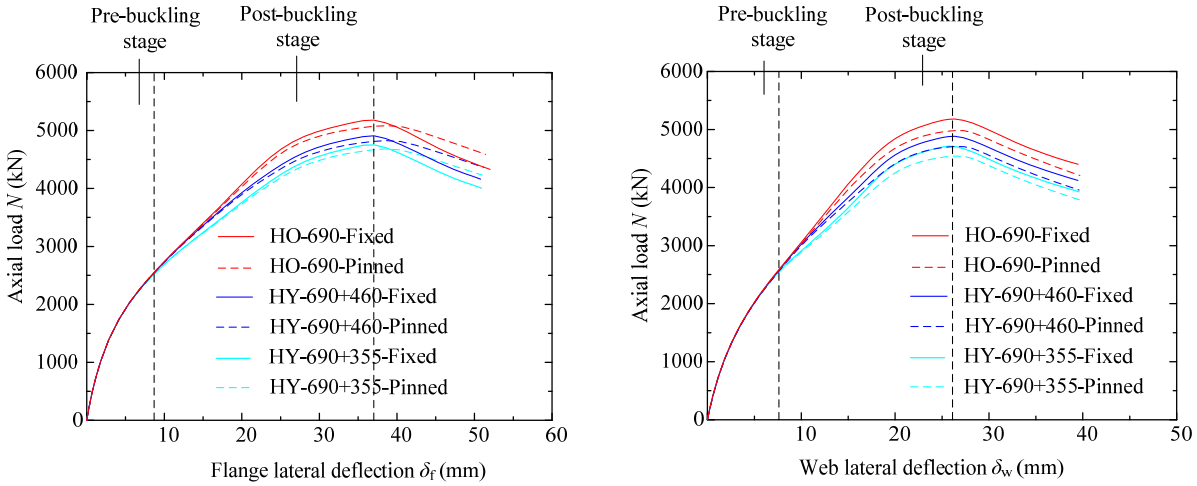

(a) "B420-H260" models (b) "B420-H440" models

Fig. 11. Axial load-lateral deflection curves of the selected I-sections with $N_u < N_y$

Normalised axial loads against end shortening δ_u of all the representative I-sections with $N < N_y$ are given in **Fig. 12**. It can be identified from these figures, N/N_y-δ_u curves is primarily dependent on the critical plate element: for models with the flange as critical plate, I-sections with different webs show similar curve response; whilst for models with the web as critical plate, lower value of N_u/N_y is achieved by I-sections with higher strength web. This is because that when the web plate failed by elastic local buckling, there is only limited contribution from the increase of web strength, but the yield load N_y of I-sections (calculated by Equation (3)) with high strength web in itself is greater than those with lower strength web.

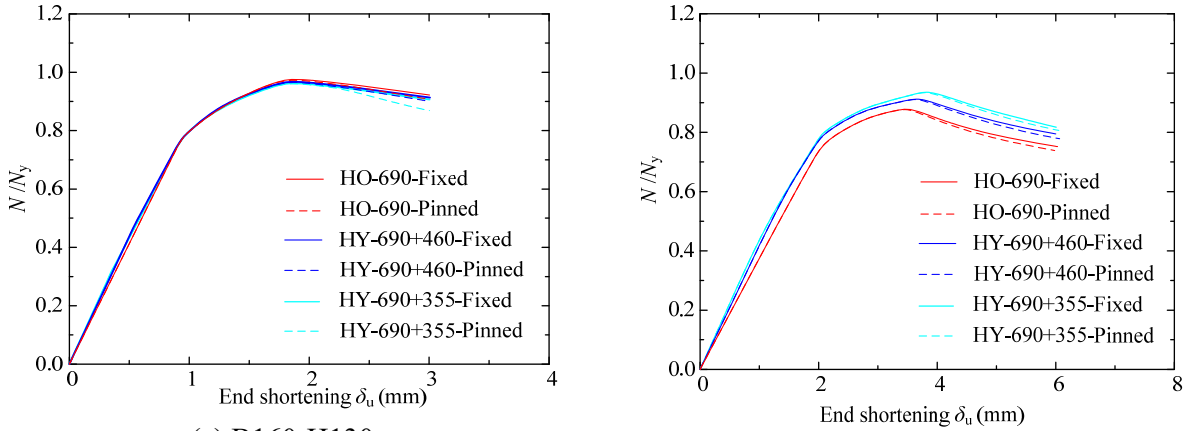

(a) B160-H130 (b) B160-H260

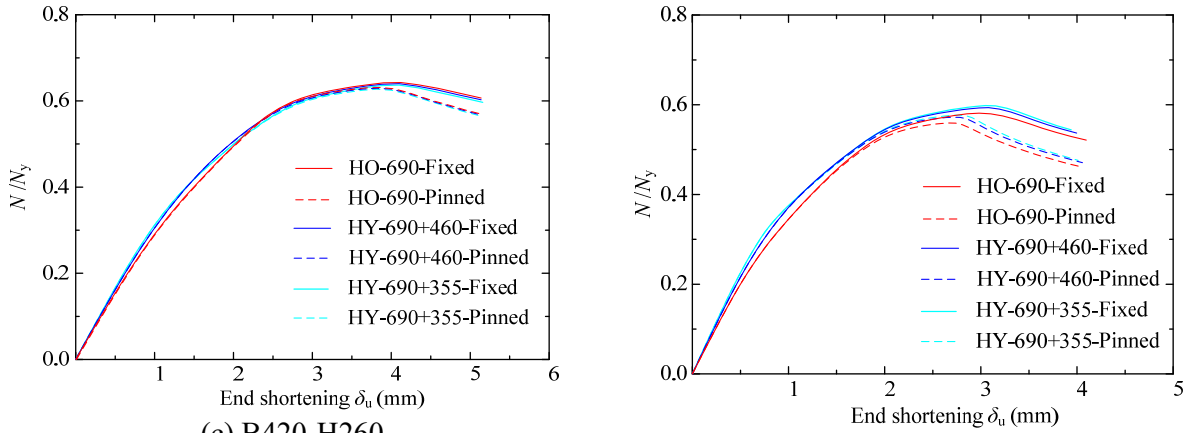

Fig. 12. Normalised axial loads against end shortening δ_u of all the representative I-sections with $N < N_y$

3.2 Effect of boundary condition

Pinned-ended boundary condition was simulated herein to explore the effect of boundary condition of the loaded edges on the local buckling behaviour of I-sections in compression. As shown in **Fig. 13**, the rotational freedom along the major and minor axis, as well as the translational freedom along the longitudinal direction of both end sections are allowed for pinned-ended I-sections.

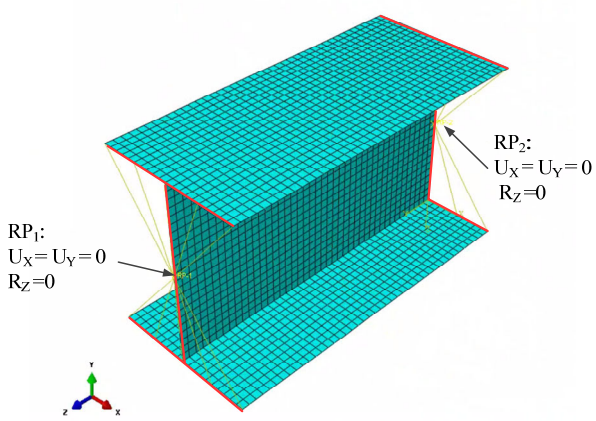

Fig. 13. Boundary condition of pinned-ended I-section models

Table 5 compares the normalised ultimate loads between fixed-ended and pinned-ended models of the selected representative I-sections. For "B80-H70" I-sections, it is interesting to see that though "HY-690+355" pinned-ended model is failure by local-overall interactive buckling (**Fig. 14(a)**), it still gives higher compression resistance than the corresponding fixed-ended model with local buckling failure mode (**Fig. 14(b)**). It can be attributed to the fairly compact plate elements of "B80-H70" I-sections, which still go into the plasticity under the condition of interactive buckling, and

unlike the fixed-ended I-sections, the web of pinned-ended models is no longer affected by the local deformation of the flange plates.

Table 5. Normalised ultimate load of the selected representative I-sections

Specimen	N_u/N_y					
	Fixed-ended			Pinned-ended		
	"HO-690"	"HY-690+460"	"HY-690+355"	"HO-690"	"HY-690+460"	"HY-690+355"
B80-H70	1.099	1.101	1.079	1.096	1.097	1.101
B160-H130	0.978	0.970	0.965	0.973	0.965	0.961
B160-H260	0.876	0.909	0.932	0.876	0.911	0.934
B420-H260	0.648	0.641	0.638	0.631	0.629	0.627
B420-H440	0.581	0.593	0.598	0.560	0.572	0.577

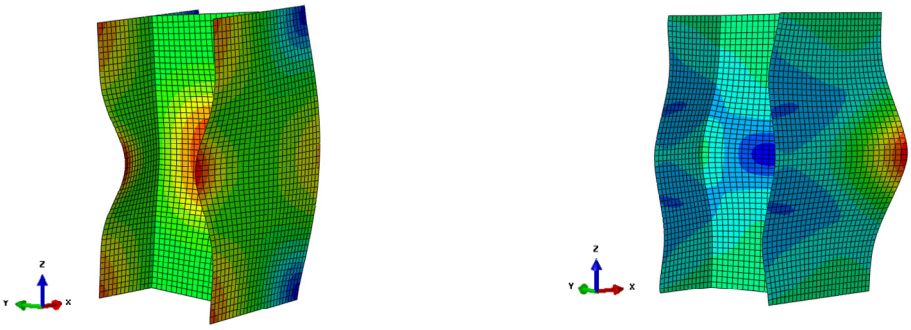

(a) Pinned-ended (b) Fixed-ended

Fig. 14. Failure modes of "B80-H70" models with different boundary conditions

(a) Pinned-ended (b) Fixed-ended

Fig. 15. Failure modes of "B160-H130" models with different boundary conditions

Among I-sections with $N_u/N_y < 1$, the failure mode of pinned-ended "B160-H130" and "B160-H260" columns with $L=3b_o$ is the same as to that with that of fixed-ended models, as provided in **Fig.15**, which is line with their close curves of N/N_y in **Fig. 12** and comparative values of N_u/N_y in **Table 5**. In addition, for "B420-H260" and "B420-H440" I-sections with elastic locally buckled critical plate, as illustrated in **Fig. 11**, the pre-buckling path of critical plate is not affected by the boundary condition of the loaded edges, though the ultimate axial loads of pinned-ended I-sections are lesser because of the occurrence of interactive buckling. Also, it was observed that the influence of web strength grade on the normalised axial load for pinned-ended I-sections was similar to those with fixed-ended boundary condition.

Overall, compared with fixed-ended models, pinned-ended I-sections are more susceptible to overall buckling, and less impacted by the local deformation of critical plate element. No distinction in the compression resistance between locally buckled pinned-ended and fixed-ended models are observed.

3.3 Effect of plate slenderness

The effect of geometric dimension-flange and web slenderness on the local buckling behaviour of I-sections under axial compression is examined underpinned by finite element results. **Fig. 16** illustrates the variation of normalised ultimate loads $N_{u,FE}/N_y$ among I-sections with different web strength grades. Models with selected flange width-to-thickness ratio b_f/t_f = 5, 10 and 21 were analysed, as presented in **Fig. 16(a)**. It can be seen from this figure that when b_f/t_f is 5, close values of $N_{u,FE}/N_y$ were observed among I-sections with different webs. For I-sections with b_f/t_f equal to 10 and 21, with the increase of web height to-thickness ratio h_w/t_w, the divergence in $N_{u,FE}/N_y$ among models with different webs was detected to be larger. This is because when the web becomes slender, it would be prone to be the critical plate element of I-sections, and thus greatly influence the values of $N_{u,FE}/N_y$. Similar observation was found for I-sections with h_w/t_w = 40 in **Fig. 16(b)**, whereas the effect of web strength grade is minor when h_w/t_w = 6.7 or 20.

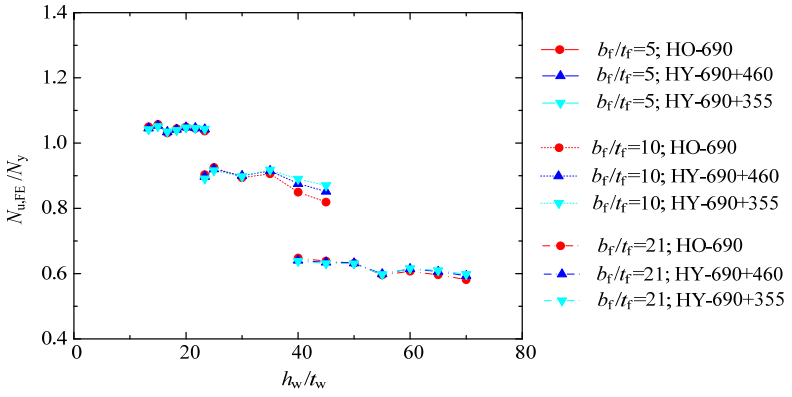

(a) Against web height-to-thickness ratio

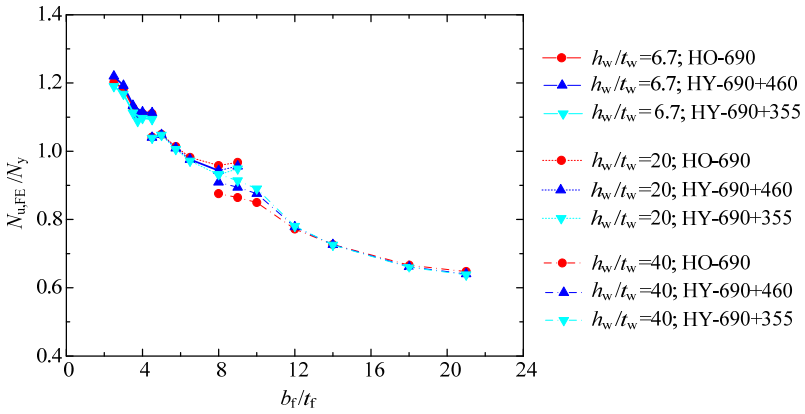

(b) Against flange width-to-thickness ratio

Fig. 16. Variation of normalised ultimate loads among I-sections with different web strength grades

It is worth noting that in the current codified design approaches for steel structures (EN 1993-1-1, 2005; ANSI/AISC 360-16, 2016; AS 4100, 2020), in terms of cross-section behaviour, the plate slenderness is stipulated together with the material yield strength by $\sqrt{f_y}$. In view of this, **Fig. 17** shows the normalised ultimate loads against $h_w/t_w \times \sqrt{f_{yw}}$ for I-sections which have been compared in **Fig. 16(a)**. Generally, it can be observed that similar trend was found among $N_{u,FE}/N_y$ against $h_w/t_w \times \sqrt{f_{yw}}$ for I-sections with different webs in **Fig. 17**.

In addition, from **Figs. 16** and **17**, it can be seen that distinct $N_{u,FE}/N_y$ results are observed among I-sections of which one plate slenderness is identical and the other plate slenderness is different, further confirming the interactive effect between flange and web plates.

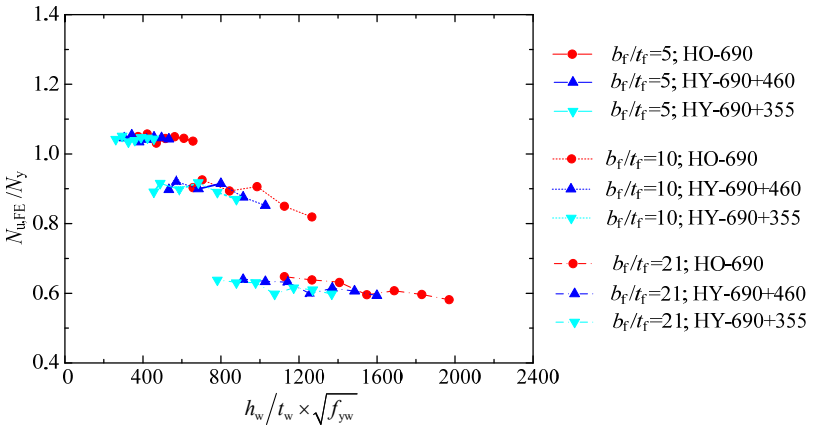

Fig. 17. Variation of normalised ultimate loads against $h_w/t_w \times \sqrt{f_{yw}}$ for I-sections with different web strength grade

3.4 Summary

Through the above parametric analysis on web strength grade, boundary condition and plate slenderness, it was shown that:

(1) The inelastic and elastic local buckling behaviour of HSS and hybrid I-sections are highly dependent on the critical plate element.

(2) Fixed-ended boundary condition, providing the comparative results to locally buckled pinned-ended models, is preferable to analyse the local buckling behaviour of I-sections under axial compression, because of the less likelihood of overall buckling.

(3) The interactive effect between flanges and web is demonstrated to exist in I-sections under axial compression.

4. Assessment on the current design methods

4.1 General

In this section, the applicability of codified design provisions based on the effective width method-European, Australian and American standards for steel structures to the design of HSS and hybrid I-section in compression was assessed, in terms of class-section classification and design resistance. Furthermore, the newly developed direct strength method (DSM) and the continuous strength method (CSM), as well as Kato's method (1998; 1999) were extended to the design of local buckling behaviour of HSS and hybrid I-sections in compression, based on the finite element results in this study, along with test data of HSS and hybrid I-sections made of 690 MPa flange in Rasmussen and Hancock (1992), Yun et al. (2021), Sun et al. (2019) and Chen et al. (2023a) described in introduction.

4.2 Effective width method

The concept of effective width (b_{eff} in **Fig. 18**), first established by Karman (1932), is used to account for the uneven stress distribution (solid line in **Fig. 18**) of buckled thin flat plate with the width of b_{p} subject to compression. This concept has been taken as the mainstream in the current design specifications of steel structures. The provisions in Eurocode 3 (EN 1993-1-1:2005, 2005; EN 1993-1-12:2007, 2007; prEN 1993-1-1:2020, 2020), Australian code (AS 4100-2020, 2020) and American specifications for steel structures (ANSI/AISC 360-16; 2016), all of which are characterised with the effective width method, were assessed in this study.

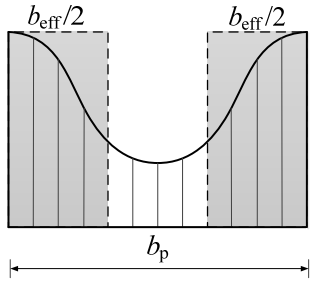

Fig. 18. Concept of effective width

400

401 **Table 6** tabulates the slenderness parameters and limiting ratios of flange (outstand compression
402 element) and web (internal compression element) in codes. The symbols in this table have been
403 illustrated in **Fig. 1**. What stands out in this table is that the limiting ratio for flange plate in
404 ANSI/AISC 360-16 (2016) uses a web slenderness-related coefficient k_c to incorporate the element
405 interaction. Plate elements with width-to thickness ratio less than the limiting ratios in this table are
406 considered to be unbuckled before yielding, and thus the full width of plate is able to reach the
407 yielding stress f_y. In **Table 6**, ε_{EC3}, ε_{AS} and ε_{AISC} represent the f_y-dependent factor in the design
408 specifications.

409

410 **Table 6.** Element classification for the I-section subject to compression in codes

Specification	f_y-dependent factor	Outstand element-flange		Internal element-web	
		Slenderness parameter	Limiting ratio	Slenderness parameter	Limiting ratio
Eurocode 3	$\varepsilon_{EC3}=\sqrt{235/f_y}$	$c_f/(\varepsilon_{EC3}t_f)$	14	$c_w/(\varepsilon_{EC3}t_w)$	42 (38 [a])
AS 4100	$\varepsilon_{AS}=\sqrt{250/f_y}$	$(b_f-t_w)/(2\varepsilon_{AS}t_f)$	14	$h_w/(\varepsilon_{AS}t_w)$	35
ANSI/AISC 360	$\varepsilon_{AISC}=\sqrt{E/f_y}$	$b_f/(2\varepsilon_{AISC}t_f)$	$0.64\sqrt{k_c}$ [b]	$h_w/(\varepsilon_{AISC}t_w)$	1.49

411 Note:

412 a. 38 is the limiting ratio in the revised version of Eurocode 3-prEN 1993-1-1:2020.

413 b. $k_c=4/\sqrt{h_w/t_w}$, but shall not be taken less than 0.35 nor greater than 0.76 for calculation purposes.

414

415 The applicability of the classification limits in Eurocode 3 to HSS and hybrid I-section stub columns
416 was set out in **Fig. 19**. Seen from **Fig. 19(a)**, the local buckling behaviour of flange plate in HSS and
417 hybrid I-sections can be generally captured by the slenderness limiting ratio-14. The web limiting
418 ratios in current version (EN 1993-1-1:2005, 2005)-42 and prEN 1993-1-1: 2020 (2020)-38 were
419 evaluated in **Fig. 19(b)**. Some data points within between 38 and 42 are below the reference line of

N_u/N_y =1 due to the element interaction, the limit in prEN 1993-1-1 (2020) is thus thought to be comparatively safter.

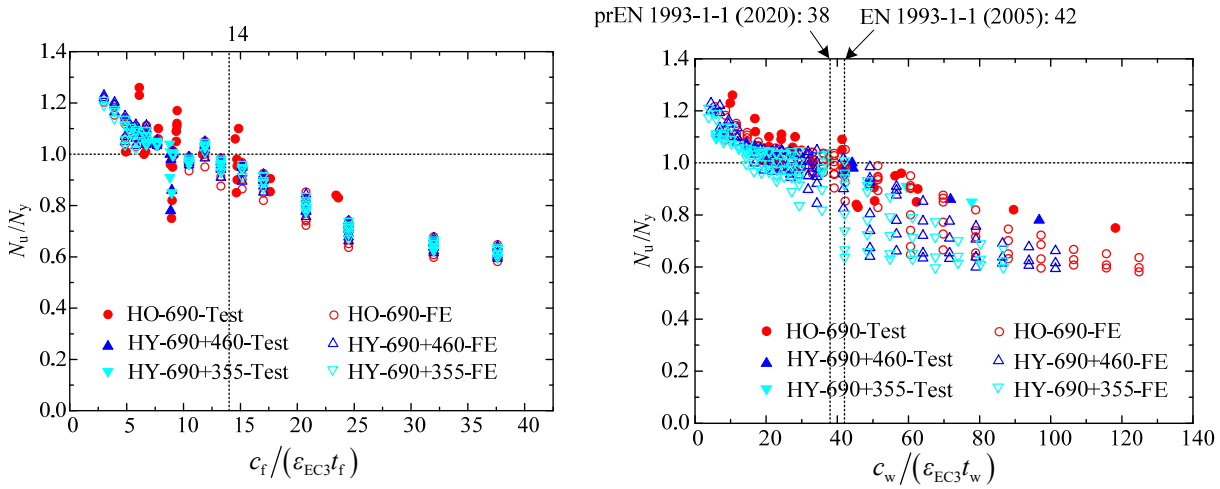

(a) Flange (b) Web

Fig. 19. Assessment of cross-section classification limit in (pr) EN1993-1-1

The predicted to-(test or) FE resistance ratios $N_{u,\,EC3}$ based on Eurocode 3 to N_u against flange and web slenderness parameters are plotted in **Fig. 20**. What is illustrated in **Fig. 20(a)** is that Eurocode 3 underestimates the compressive resistance of HSS and hybrid I-sections with slender flange, which agrees with the findings of Shi et al. (2014; 2015) for Q460 and Q960 welded I-sections in compression, implying that those codified design expressions in Eurocode 3 (EN 1993-1-5:2006, 2006) gives conservative results for outstand compression elements. Fairly scattered prediction results of $N_{u,EC3}/N_u$ were observed for I-sections with high web slenderness ratio, as shown **Fig. 20(b)**, which demonstrates that flange width-to-thickness ratio affects the prediction accuracy of I-sections with identical web slenderness, principally attributed to the interactive effect between flanges and web.

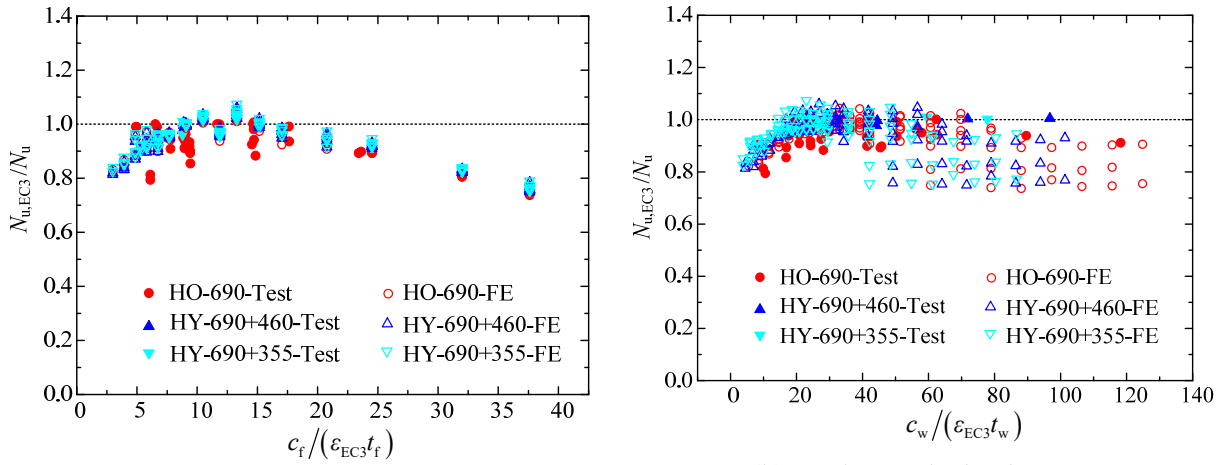

(a) Against flange slenderness

(b) Against web slenderness

Fig. 20. Comparison of normalised ultimate loads between (test or) finite element results and design resistances in Eurocode 3

Figs 21 and 22 show the assessment results of Australian code (AS4100-2020, 2020). Which is displayed in **Fig. 21** is that the yield slenderness limiting ratios in AS4100 are acceptable to classify the local buckling behaviour for flange and web elements of HSS and hybrid I-sections. The ratios of Australian code prediction results $N_{u,AS}$ to test and FE data N_u against flange and web slenderness were shown in **Fig. 22**. Similar observation results to Eurocode 3 were obtained: underpredicted compression resistances were found for sections with high slenderness flange, and scattered predictions was given by slender-web sections.

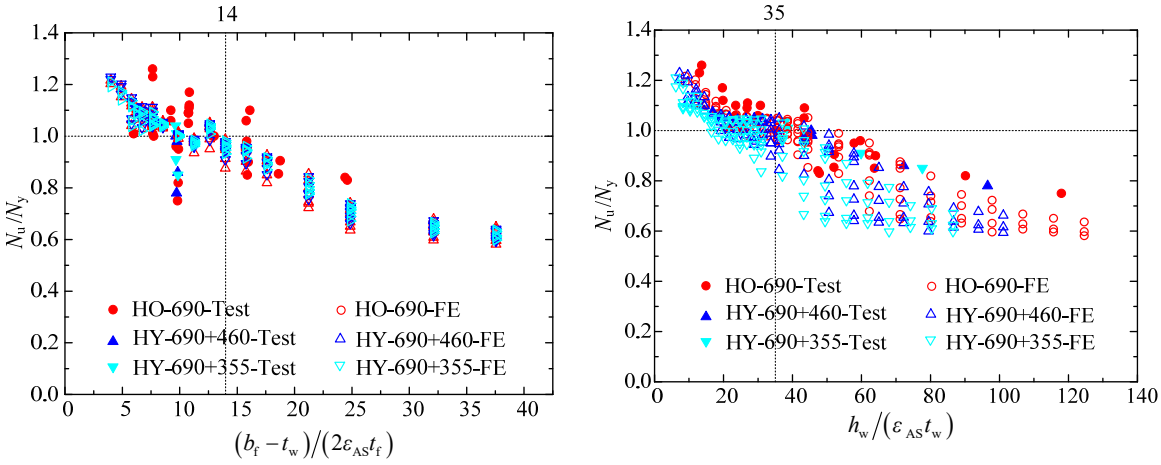

(a) Flange

(b)Web

Fig. 21. Assessment of cross-section classification limit in AS 4100

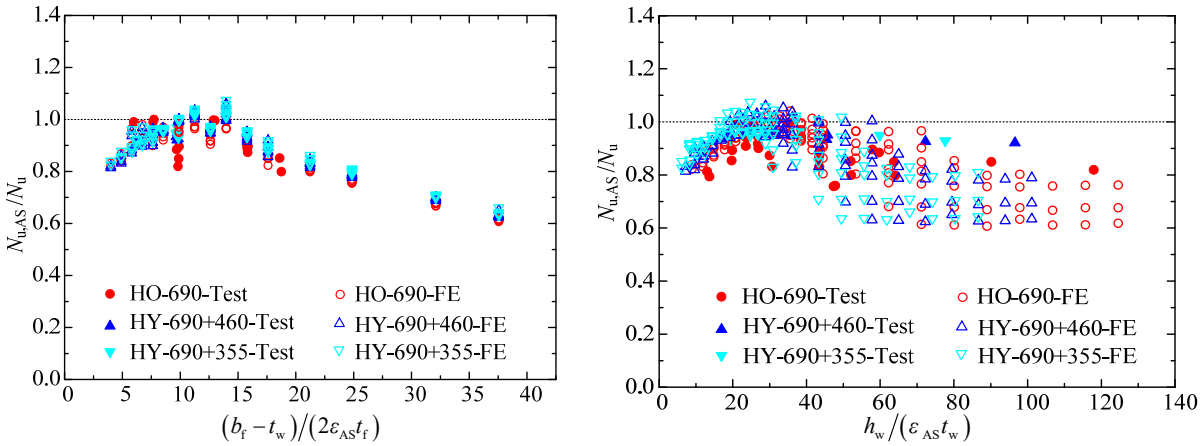

(a) Against flange slenderness (b) Against web slenderness

Fig. 22. Comparison of normalised ultimate loads between (test or) finite element results and design resistances in AS 4100

The slenderness limitations in ANSI/AISC 360 (2016) based on the test and FE data set were assessed in **Fig. 23**. In **Fig. 23(a)**, the flange slenderness limit is expected to be stricter for HSS and hybrid I-sections to provide safe predictions, and **Fig. 23(b)** reveals that the limiting ratio of web plate is suitable for investigated I-sections. The predicted-to-test (or FE) resistance ratios $N_{u,AISC}/N_u$ based on ANSI/AISC 360-16 is given in **Fig. 24**. It was clear that the AISC provisions generally offer accurate predictions, but some overestimated results might lead to unsafe design for HSS and hybrid I-sections.

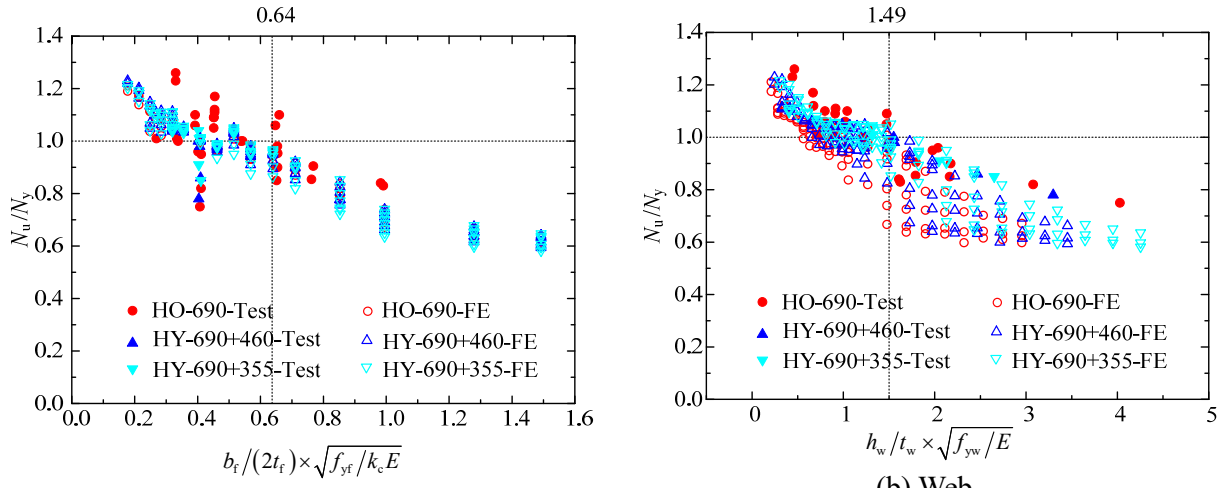

(a) Flange (b) Web

Fig. 23. Assessment of cross-section classification limit in ANSI/AISC 360

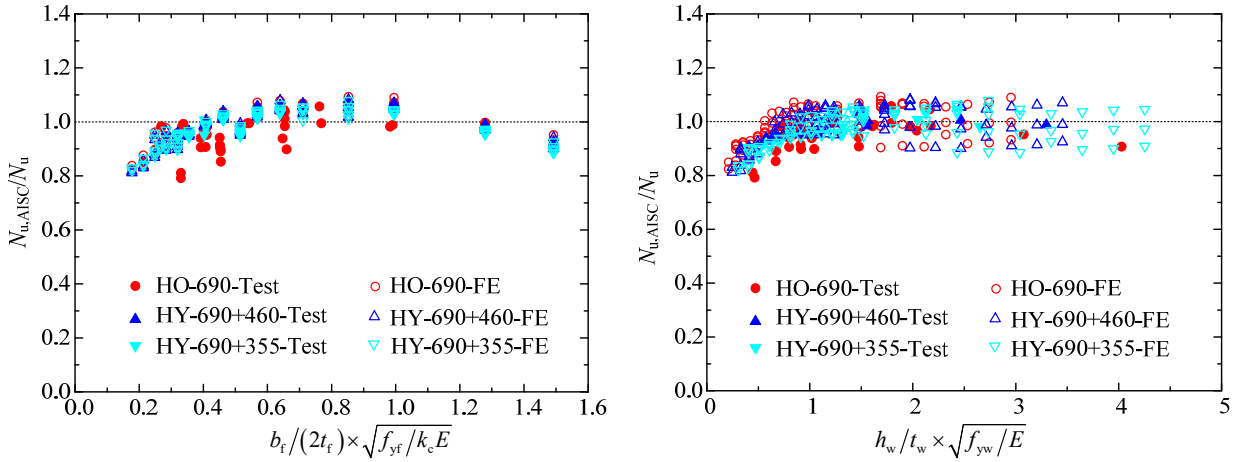

(a) Flange (b) web

Fig. 24. Comparison of normalised ultimate loads between (test or) finite element results and design resistances based on ANSI/AISC 360

In general, the slenderness limits in European, Australian and American codes are suitable for welded HSS and hybrid I-sections in compression. Eurocode 3 and AS 4100 give overconservative predictions to I-sections with slender flange, in comparison, AISC specification provides more accurate predictions.

4.3 Direct strength method

Distinct from the effective width method, the direct strength method (DSM) is based on the overall cross-section slenderness λ_p, rather than individual plate slenderness, to take account of the flange-web interaction. The overall cross-section slenderness λ_p can be calculated by Equation (4), where, the second expression which is load-dependent can be taken as $\lambda_{p,N}$.

$$\lambda_p = \begin{cases} \sqrt{\dfrac{f_y}{f_{cr,cs}}} & \text{stress-dependent} \\ \text{or} & \\ \sqrt{\dfrac{N_y}{N_{cr,cs}}} = \sqrt{\dfrac{N_y}{f_{cr,cs}\times A_{cs}}} = \lambda_{p,N} & \text{load-dependent} \end{cases} \tag{4}$$

In this equation, $f_{cr,cs}$ and $N_{cr,cs}$ denote the critical elastic buckling stress and load of overall cross-section, and A_{cs} represent the gross cross-section area. The value of $\sigma_{cr,cs}$ can be determined by finite element or finite strip methods, as well as estimated formulae. In this study, the calculation of $f_{cr,cs}$ is based on the estimation approach proposed by Gardner et al. (2019). It is worth noting that for homogenous sections with single one steel material, the result of stress-dependent expression in Equation (4) is the same as the load-dependent one. However, for hybrid sections consisting of

different steel materials, there could be different considerations on the selection of f_y in Equation (4). According to the comprehensive parametric study results in Section 3, the local buckling behaviour of hybrid I-sections is highly dependent on the critical plate element which governs the local instability behaviour. Therefore, for hybrid I-sections, the stress-dependent expression in Equation (4) At the same time, load-dependent overall cross-section slenderness is also considered in the following analysis.

The DSM utilises the direct relation between the design resistance and overall cross-section slenderness, and it has been applied to design of the cold-formed, hot-rolled and welded HSS sections (Shifferaw and Schafer, 2012; Pham and Hancock; 2013; Li, 2014; Chen et al., 2022). Li (2014) extended the DSM to the design of welded homogeneous H-sections made of 235 MPa, 355 MPa and 460 MPa steels, whose formulas are indicated by Equation (5).

$$\frac{N_{u,DSM,Li}}{N_y}=\begin{cases}1 & \lambda_p \le 0.694\\ \dfrac{0.499}{\lambda_p^{0.465}}+\dfrac{0.29}{\lambda_p^{0.93}} & \lambda_p > 0.694\end{cases} \tag{5}$$

Fig. 25(a) depicts the relation between N_u/N_y and stress-dependent overall cross-section slenderness based on the critical plate $\lambda_{p,cr}$ of all the test and FE data. It was shown that the equations developed by Li (2014) can generally capture the local buckling behaviour of HSS and hybrid I-sections. However, data points belong to "HY-690+355" slender I-sections with $\lambda_{p,cr} > 0.694$ were found to be located below the Li's DSM curve. This is because the lower strength web resulting to the lesser value of $\lambda_{p,cr}$ when web plate is critical.

The ratio of N_u to N_y against load-dependent overall cross-section slenderness $\lambda_{p,N}$ is presented in **Fig. 25(b)**, where more concentrated distribution data were detected among slender I-sections, but underestimated by Li's curve. Thus, it is suggested to establish a new DSM curve based on the load-dependent slenderness $\lambda_{p,N}$ for the investigated HSS and hybrid I-sections, as expressed by Equation (6), which has been shown to fit the data points well in **Fig. 25(b)**.

$$\frac{N_{u,DSM}}{N_y}=\begin{cases}1 & \lambda_{p,N} \le 0.68\\ \left(1-0.165\times\lambda_{p,N}^{-0.63}\right)\times\lambda_{p,N}^{-0.63} & \lambda_{p,N} > 0.68\end{cases} \tag{6}$$

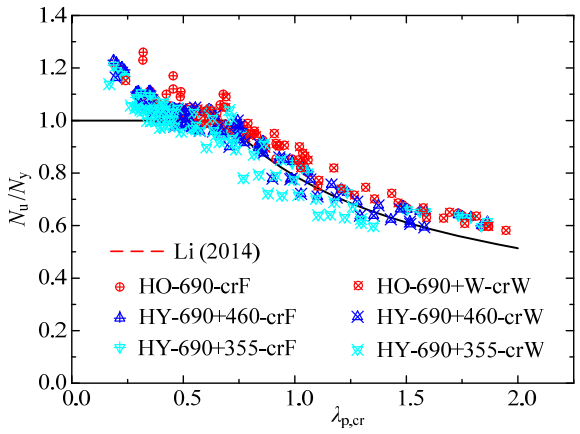

(a) Against stress-dependent overall cross-section slenderness

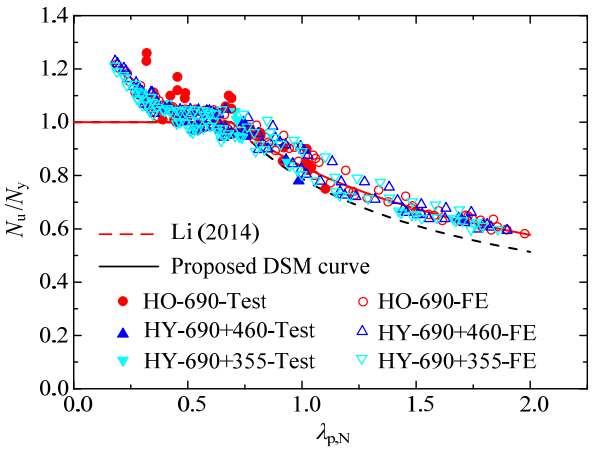

(b) Against load-dependent overall cross-section slenderness

Fig. 25. Normalised ultimate load against the overall cross-section slenderness curves

4.4 Continuous strength method

The continuous strength method (CSM) is a deformation-based design method, incorporating the deformation ability and material properties of the whole cross-section. In this method, the deformation capacity is featured by the base curve, which describes the correlation between the ratio of the CSM limiting strain to yield strain-$\varepsilon_{CSM}/\varepsilon_y$ and the overall cross-section slenderness λ_p; an appropriate material model is also indispensable to transform ε_{CSM} to the CSM limiting stress f_{CSM}, so that the cross-section resistance can be derived by stress distribution. The expressions for the CSM base curve for non-slender and slender sections have been developed for materials with an obvious yield plateau (Buchanan et al., 2016; Zhao et al., 2017), as denoted by Equation (7); then using the constitutive relation between f_{CSM} and ε_{CSM} (Equation (8)), the compression strength can be obtained by Equation (9).

$$\frac{\varepsilon_{CSM}}{\varepsilon_y}=\begin{cases}\dfrac{\delta_u/L}{\varepsilon_y}\le \min\left(15,\dfrac{C_1\varepsilon_u}{\varepsilon_y}\right) & \text{for non-slender sec tions}\\ \dfrac{N_u}{N_y} & \text{for slender sec tions}\end{cases} \tag{7}$$

$$f_{CSM}=\begin{cases}E\varepsilon_{CSM} & \text{for } \varepsilon_{CSM}\le\varepsilon_y\\ f_y & \text{for } \varepsilon_y<\varepsilon_{CSM}\le\varepsilon_{sh}\\ f_y+E_{sh}\left(\varepsilon_{CSM}-\varepsilon_{sh}\right) & \text{for } \varepsilon_{sh}<\varepsilon_{CSM}\le C_1\varepsilon_u\end{cases} \tag{8}$$

$$N_{CSM}=Af_{CSM} \tag{9}$$

The material model parameters for HSSs have been developed in Chen et al. (2022) based on the quad-linear stress-strain relation for hot-rolled steels proposed by Yun and Gardner (2017), which is illustrated in **Fig. 26**. Where, C_1 is the model coefficient applied in Equation (7) to avoid over-

strength predictions, and C_2 is used to determine strain hardening modulus E_{sh}. The formulas of ε_u, ε_{sh}, C_1 and C_2 for HSS and hot-rolled steels can be found in Chen et al. (2022) and Yun and Gardner (2017).

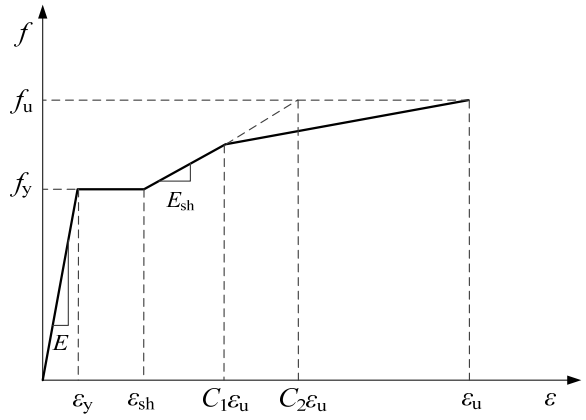

Fig. 26. Quad-linear material model for HSS materials in the CSM

Based on the above Equations (7)~(9), for slender I-sections, the CSM compressive resistance expression for slender I-sections is obtained by regressively analysing the ratios of N_u to N_y. Thus, the design expression for slender I-sections with $\lambda_{p,N} > 0.68$ in the DSM can be directly applied to the base curve for slender sections in the CSM with high accuracy, as set out in **Fig. 27**.

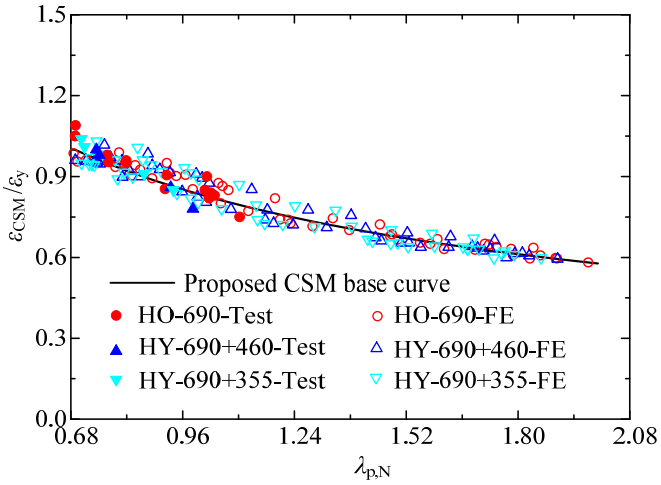

Fig. 27. Base curve for slender I-sections in the CSM

As presented by Equation (7), the deformation ability, i.e., base curve for non-slender I-sections, is denoted by the ratio of normalised end shortening δ_u/L at the ultimate load N_u of columns to the yield strain δ_y. **Fig. 28** presents the normalised end shortening δ_u/L against stress-dependent and load-dependent overall cross-section slenderness-$\lambda_{p,cr}$ and $\lambda_{p,N}$. It can be observed from **Fig. 28(a)** that only minor differences in deformation δ_u/L were found among non-slender web-critical I-sections, whilst distinct values of $\lambda_{p,cr}$ are obtained because of different web yield strength. Compared with $\lambda_{p,cr}$, less dispersed data distribution could be obtained by using $\lambda_{p,N}$ as the abscissa, as shown in **Fig. 28(b)**.

This result can be explained by that though the local buckling behaviour of I-sections in compression is significantly affected by the critical plate element of I-sections, only minor distinctions in the ultimate loads among I-sections with different webs were observed, as shown by the curves of **Figs 8, 12, 16** and the data of **Table 5**. In **Fig. 28(a)**, "-crF" and "-crW" mean these models are featured with flanges and web as the critical plates, respectively.

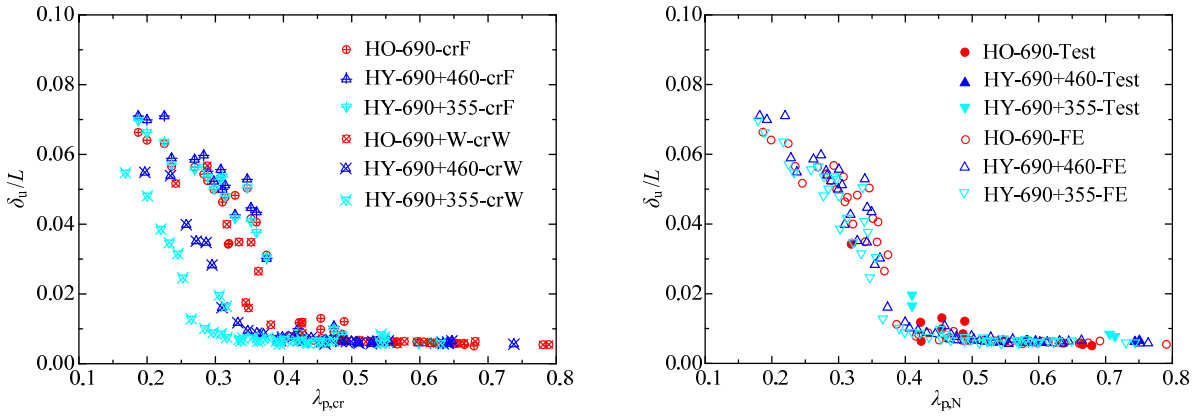

(a) Against stress-dependent overall cross-section slenderness

(b) Against load-dependent overall cross-section slenderness

Fig. 28. Deformation of non-slender HSS and hybrid I-sections against overall cross-section slenderness

The deformation capacity of HSS and hybrid I-sections against the stress-dependent and load-dependent overall cross-section slenderness is depicted in **Fig. 29(a) and (b)**. In this figure, $\varepsilon_{y,cr}$ is the yield strain of critical plate element of I-sections; $\varepsilon_{y,aver}$ denotes the area-weighted average yield strain, which is the ratio of area-weighted average yield strain $f_{y,aver}$ to the elastic modulus E, as expressed by Equation (10).

$$\varepsilon_{y,aver} = \frac{f_{y,aver}}{E} = \frac{N_y / A_{cs}}{E} \tag{10}$$

Lan et al. (2018) and Liu et al. (2023) established the CSM base curves for non-slender HSS rectangular/square hollow sections (Equation (11)) and hybrid T-sections with Q690 flange and Q355 web (Equation (12)), respectively. The deformation ability of HSS and hybrid I-sections against the stress-dependent slenderness of critical plate was compared with the curves of Lan et al. (2018) and Liu et al. (2023) in **Fig. 29**. From **Fig. 29(a)**, it can be seen that the scatteredly distributed data points based on the critical plate of I-sections cannot be captured well by Equations (11) and (12). In **Fig. 29(b)**, when the load-based overall cross-section slenderness $\lambda_{p,N}$ is used, it was found that both of Lan et al. (2018) and Liu et al. (2023) curves largely overpredict the deformation ability of non-

slender I-section with $\lambda_{p,N} > 0.37$, and thus a new CSM base curve for HSS and hybrid I-sections in compression based on $\lambda_{p,N}$ was developed, whose expression is denoted by Equation (13).

$$\left(\frac{\varepsilon_{CSM}}{\varepsilon_y}\right)_{Lan} = \frac{0.294}{\lambda_p^{3.174}} \le \min\left(15, \frac{C_1\varepsilon_u}{\varepsilon_y}\right) \quad \text{for } \lambda_p \le 0.68 \tag{11}$$

$$\left(\frac{\varepsilon_{CSM}}{\varepsilon_y}\right)_{Liu} = \frac{0.178}{\lambda_p^{3.887}} \le \min\left(15, \frac{C_1\varepsilon_u}{\varepsilon_y}\right) \quad \text{for } \lambda_p \le 0.64 \tag{12}$$

$$\frac{\varepsilon_{CSM}}{\varepsilon_y} = \begin{cases} \dfrac{0.33}{\lambda_{p,N}^{2.9}} \le \min\left(15, \dfrac{C_1\varepsilon_u}{\varepsilon_y}\right) & \text{for } \lambda_{p,N} \le 0.68 \\ \left(1 - 0.165 \times \lambda_{p,N}^{-0.63}\right) \times \lambda_{p,N}^{-0.63} & \text{for } \lambda_{p,N} > 0.68 \end{cases} \tag{13}$$

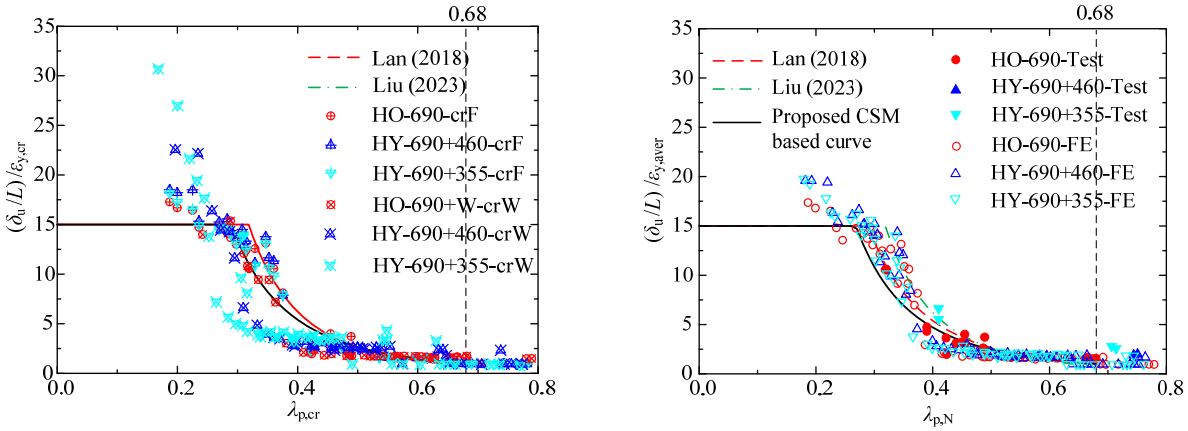

(a) Against stress-dependent overall cross-section slenderness

(b) Against load- dependent overall cross-section slenderness

Fig. 29. Base curve for non-slender HSS and hybrid I-sections in the CSM

Based on the obtained the CSM base curve (Equation (13)) and the quad-linear material model in **Fig. 26**, the compression resistance of HSS and hybrid I-section stub columns can be obtained according to Equations (7)~(9). Note that for I-sections fabricated by different steels, Equation (9) needs to be converted into Equation (14), where $f_{CSM,f}$ and $f_{CSM,w}$ represent the CSM limiting stresses of flange and web plates, respectively. The CSM material model for HSS (Q690 and Q460 in this study) and NSS (Q355 in this study) plate elements can refer to Chen et al. (2022) and Yun and Gardner (2017).

$$N_{CSM} = A_f \times f_{CSM,f} + A_w \times f_{CSM,w} \tag{14}$$

4.5 Kato's method

The method proposed by Kato (1998, 1999) is adopted to be the basis of cross-section classification in the Japanese recommendation for limit state design of steel structures (AIJ LSD, 2010), which has

specified the design of I-/H-section structural steels with $f_{y,nom}$ up to 440 MPa. According to Kato's method, the cross-section resistance in compression can be expressed by Equation (15), where, A, B and C are the coefficients to be determined on the statistics analysis of data; λ_f and λ_w denote flange slenderness and web slenderness, which can be calculated using Equation (16). It can be seen from these equations, this method incorporates the flange and web slenderness into one equation to consider the element interaction.

$$\frac{1}{N_{Kato}/N_y} = A + \frac{B}{\lambda_f} + \frac{C}{\lambda_w} \tag{15}$$

where,

$$\begin{cases} \lambda_f = \dfrac{E}{f_{yf}}\left(\dfrac{t_f}{b_f/2}\right)^2 \\ \lambda_w = \dfrac{E}{f_{yw}}\left(\dfrac{t_w}{h_w}\right)^2 \end{cases} \tag{16}$$

After a statistical analysis of the data pool in this study, the design compressive resistance based on the Kato's method can be obtained as Equation (17). By substituting $N_{u,Kato} = N_y$ into Equation (17), the classification limit is thus derived as Equation (18). As a result, Equation (19) is then taken as the design equations for HSS and hybrid I-section under axial compression. **Fig. 30** compares the test and FE results with the proposed Kato's curve, this curve was observed to provide satisfactory results.

$$\frac{1}{N_{u,Kato}/N_y} = 0.954 + \frac{0.343}{\lambda_f} + \frac{0.019}{\lambda_w} \tag{17}$$

$$\left(\frac{b_f/2t_f}{0.37\times\sqrt{E_f/f_{yf}}}\right)^2 + \left(\frac{h_w/t_w}{1.56\times\sqrt{E_w/f_{yw}}}\right)^2 = 1 \tag{18}$$

$$\frac{1}{N_{u,Kato}/N_y} = \begin{cases} 1 & \left(\dfrac{b_f/2t_f}{0.37\times\sqrt{E_f/f_{yf}}}\right)^2 + \left(\dfrac{h_w/t_w}{1.56\times\sqrt{E_w/f_{yw}}}\right)^2 \le 1 \\ 0.954 + \dfrac{0.343}{\lambda_f} + \dfrac{0.019}{\lambda_w} & \left(\dfrac{b_f/2t_f}{0.37\times\sqrt{E_f/f_{yf}}}\right)^2 + \left(\dfrac{h_w/t_w}{1.56\times\sqrt{E_w/f_{yw}}}\right)^2 > 1 \end{cases} \tag{19}$$

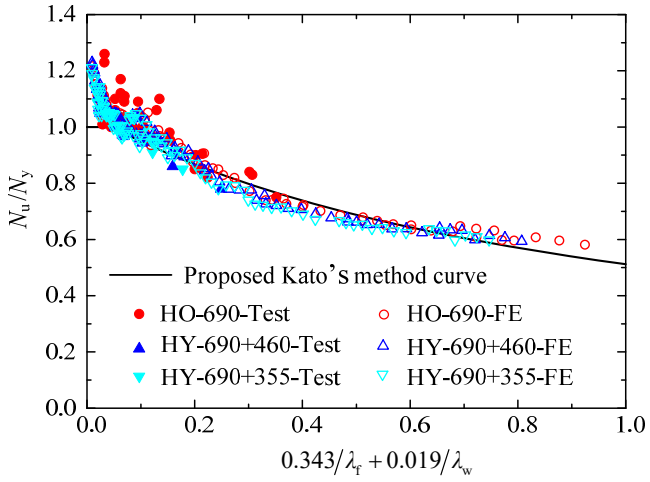

Fig. 30. Proposed curve based on the Kato's method

595

596 **4.6 Summary**

597 The statistical analysis results of the codified design methods, as well as the newly proposed DSM,
598 CSM and Kato's method expressions are summarised in **Table 7**. Among all the mentioned design
599 codes, it can be seen from this table that ANSI/AISC 360-16 (2016) offers more suitable results than
600 Eurocode 3 and AS 4100, and it was also found that these design provisions always give more
601 accurate predictions for hybrid I-sections with the lowest strength web- "HY-690+355". In addition,
602 all the newly developed design expressions provide satisfactory predictive accuracy. In comparison,
603 the CSM generally shows more accurate and less scattered predictions, which might be attributed to
604 the consideration of the strain hardening in the CSM material model, whereas both the design
605 formulas of the DSM and Kato's method take $N_{u,pred}=N_y$ for non-slender I-sections in compression.

606

607 **Table 7**. Statistical analysis results of design methods

Design method	HO-690		HY-690+460		HY-690+355	
	Mean	CoV	Mean	CoV	Mean	CoV
$N_u/N_{u,EC3}$	1.081	0.083	1.071	0.086	1.065	0.083
$N_u/N_{u,AS}$	1.160	0.141	1.141	0.146	1.128	0.143
$N_u/N_{u,AISC}$	1.036	0.066	1.023	0.067	1.019	0.063
$N_u/N_{u,DSM}$	1.040	0.055	1.031	0.058	1.026	0.057
$N_u/N_{u,CSM}$	1.042	0.052	1.034	0.053	1.030	0.051
$N_u/N_{u,Kato}$	1.055	0.055	1.036	0.059	1.027	0.058

608

609 **5 Reliability analysis**

610 The first-order reliability analysis method in Eurocode 3 (EN 1990, 2005) was adopted to assess the
611 reliability level of the treatment of local buckling behaviour for HSS and hybrid I-sections in
612 compression discussed in Section 4. The material over-strength $f_{y,mean}/f_{y,nom}$, was 1.12 with the CoV =

0.066 according to statistical results in Chen et al. (2022), and the CoV of geometric properties was selected to be 0.05 (AA ADM-2010, 2010; Chen et al., 2022). Reliability analysis results of design methods are tabulated in **Table 8**. In this table, b is the average ratio of test and FE results to design strength according to the least squares analysis; V_r means the CoV covering both model and basic variable uncertainties; γ_{M0} denotes the partial safety factor for cross-section resistance.

It is clear from this table that with the highest partial safety factors-1.24 and 1.25, Australian code (AS 4100-2020, 2020) usually overestimates the compression resistance of HSS and hybrid I-section stub columns, whereas Eurocode 3 and AISC specification present more reliable design resistance results with the derived partial factors ranging between 1.16-1.18. In comparison, all the newly proposed design expressions in this study feature lesser values of V_r and γ_{M0}, demonstrating that more accurate and less scattered predictions than the design rules in codes.

Table 8. Reliability analysis results of design methods

Design method	Section steel combination	b	V_r	γ_{M0}
Eurocode 3	HO-690	0.994	0.115	1.17
	HY-690+460	1.051	0.117	1.18
	HY-690+355	1.060	0.115	1.17
AS 4100	HO-690	1.117	0.156	1.24
	HY-690+460	1.080	0.160	1.25
	HY-690+355	1.060	0.156	1.24
ANSI/AISC 360	HO-690	0.963	0.105	1.16
	HY-690+460	1.025	0.106	1.16
	HY-690+355	1.020	0.104	1.16
DSM	HO-690	1.047	0.099	1.15
	HY-690+460	1.036	0.099	1.15
	HY-690+355	1.027	0.099	1.15
CSM	HO-690	1.048	0.097	1.15
	HY-690+460	1.040	0.098	1.15
	HY-690+355	1.036	0.097	1.15
Kato	HO-690	1.062	0.099	1.15
	HY-690+460	1.045	0.101	1.15
	HY-690+355	1.036	0.101	1.15

6 Conclusions

This study focuses on the local buckling behaviour of welded HSS and hybrid I-sections under axial compression, which has not been dealt with in detail in previous literature. Using the validated numerical method, an extensive parametric study was conducted to investigate the effect of web

strength grade, boundary condition and plate slenderness. The parametric study results revealed that the critical plate element governs the local buckling behaviour of HSS and hybrid I-sections. The interactive effect between flanges and web is also confirmed to exist in I-sections in compression.

A total of 243 models of HSS and hybrid I-section stub columns established in this study, as well as the collated test data, were used to assess the design rules in European, Australian, and American standards for designing steel structures. Among the codified design provisions, ANSI/AISC 360-16 was found to offer more reliable design resistance than Eurocode 3 and AS 4100. In addition, the recently developed continuous strength method (CSM), direct strength method (DSM) and Kato's method, which can consider flange-web interaction, were extended to the design of HSS and hybrid I-sections in compression. Statistical and reliability analysis results have demonstrated the satisfactory predictions of the proposed CSM, DSM, and Kato's method design expressions. These newly developed design approaches that consider flange-web interaction are expected to improve the accuracy and efficiency for the design of the local buckling behaviour of HSS and hybrid I-sections in compression. This paper provides insight into the local buckling behaviour and mechanism behind plate interaction of hybrid I-sections.

CRediT authorship contribution statement

Shuxian Chen: Writing – original draft, Investigation. Jun-zhi Liu: Writing – review & editing. Tak-Ming Chan: Writing – review & editing, Supervision, Funding acquisition.

Declaration of Competing Interest

The authors declare that they have no known competing financial interests or personal relationships that could have appeared to influence the work reported in this paper.

Acknowledgements

The finding support from the Chinese National Engineering Research Centre for Steel Construction (Hong Kong Branch) at The Hong Kong Polytechnic University is gratefully acknowledged.

Reference

Aluminium Association (2010) Aluminium Design Manual AA ADM-2010, AA, Washington, DC.

American Institute of Steel Construction (2010) Specification for Structural Steel Buildings, ANSI/AISC 360-10, AISC, Chicago, Illinois.

American Institute of Steel Construction (2016) Specification for Structural Steel Buildings, ANSI/AISC 360-16, AISC, Chicago, Illinois.

Architectural Institute of Japan (2010) Recommendation for Limit State Design of Steel Structures,

AIJ, Tokyo.
Bai, L. and Wadee, M.A. (2015) Mode interaction in thin-walled I-section struts with semi-rigid flange–web joints. International Journal of Non-Linear Mechanics. 69, 71-83.
Bedair, O. (2009) Stability of web plates in W-shape columns accounting for flange/web interaction. Thin-walled Structures. 47, 768-775.
Bleich, F. (1952) Buckling Strength of Metal Structures, McGraw-Hill, New York, NY.
British Standards Institute (2017) BS EN 10365:2017- Hot rolled steel channels, I and H sections. Dimensions and masses. BSI, London.
Buchanan, C., Gardner, L., Liew, A. (2016) The continuous strength method for the design of circular hollow sections, Journal of Constructional Steel Research. 118, 207–216.
Cao, X.L., Zhao, G., Kong, Z.Y., et al. (2020) Experimental study on local buckling of 800 MPa HSS welded I-section columns under axial compression. Thin-Walled Structures. 155, 106878.
Chen, S.X., Fang, H., Liu, J.Z., Chan, T.M. (2022) Design for local buckling behaviour of welded high strength steel I-sections under bending. Thin-Walled Structures.172, 108792.
Chen, S.X., Liu, J.Z., Chan, T.M. (2023a) Investigations into the local buckling and post-buckling behaviour of fixed-ended hybrid I-section stub columns with slender web. Thin-Walled Structures. 184, 110174.
Chen, S.X., Liu, J.Z., Chan, T.M. (2023b) Material properties and residual stresses of welded high strength steel and hybrid I-sections. Engineering Structures. 276, 115293.
European Committee for Standardization (2005) EN 1990, Eurocode - Basis of Structural Design, CEN, Brussels.
European Committee for Standardization (2005) EN 1993-1-1:2005, Eurocode 3: Design of Steel Structures - Part 1-1: General Rules and Rules for Buildings, CEN, Brussels.
European Committee for Standardization (2020) prEN 1993-1-1:2020, Eurocode 3: Design of Steel Structures - Part 1-1: General Rules and Rules for Buildings, CEN, Brussels.
European Committee for Standardization (2006) EN 1993-1-5:2006. Eurocode 3 - Design of Steel Structures - Part 1-5: Plated Structural Elements, CEN., Brussels.
European Committee for Standardization (2007) EN 1993-1-12:2007, Eurocode 3: Design of steel structures: Part 1-12: General - High strength steels, CEN, Brussels.
Fieber, A., Gardner, L., Macorini, L. (2019) Formulae for determining elastic local buckling half-wavelengths of structural steel cross-sections. Journal of Constructional Steel Research. 159, 493-506.
Gardner, L., Fieber, A., Macorini, L. (2019) Formulae for Calculating Elastic Local Buckling Stresses of Full Structural Cross-sections. Structures. 17, 2–20.
Lan, X.Y., Chen, J.B., Chan,T.M., Young, B. (2018) The continuous strength method for the design

701 of high strength steel tubular sections in compression. Engineering Structures. 162, 177–187.
702 Li, D.X., Huang, Z.C., Uy, B., Thai, H. T., Hou, C. (2019) Slenderness limits for fabricated S960
703 ultra-high-strength steel and composite columns. Journal of Constructional Steel Research, 159, 109-
704 121.
705 Li, Y.Z. (2014) Extension of the Direct Strength Method to hot-rolled and welded H profile cross-
706 sections. Ph.D. Thesis, Université de Liège, Belgium.
707 Liu, J.Z., Chen, S.X., Chan, T.M. (2023) Hybrid welded T-section stub columns with Q690 flange
708 and Q355 web: Testing, modelling and design. Engineering Structures, 115142.
709 Kármán, T. von, Sechler, E.E. and Donnell, L.H. (1932) The strength of thin plates in compression.
710 Transactions of the American Society of Mechanical Engineers. 54, 53-57.
711 Kato, B. (1998) Rotation capacity of H-section members as determined by local buckling, Journal of
712 Constructional Steel Research. 13, 95-109.
713 Kato, B. (1999) Deformation capacity of steel structures. Journal of Constructional Steel Research.
714 17, 33-94.
715 Miki, C., Homma, K., Tominaga, T. (2002) High strength and high performance steels and their use
716 in bridge structures. Journal of Constructional Steel Research. 58, 3–20.
717 NagarajaRao, N. R. (1965) The Strength of Hybrid Steel Columns. Fritz Engineering Laboratory
718 Department of Civil Engineering Lehigh University Bethlehem, Pennsylvania Fritz Laboratory
719 Report No. 305.1
720 NagarajaRao, N. R., Marek, P. and Tall, L. (1969) Hybrid steel columns. Fritz Laboratory Reports.
721 Paper 1877. Available from: http://preserve.lehigh.edu/engr-civil-environmental-fritz-lab-
722 reports/1877 [Accessed 18th May 2022]
723 Nagarajarao, N. R., Marek, P. and Tall, L. (1972) Welded Hybrid Steel Columns. Welding Research
724 Supplement, 462-472.
725 Pocock, G. (2006) High strength steel use in Australia, Japan and the US. The Structural Engineer.
726 84 (21), 27-30.
727 Rasmussen, K. J. R. & Hancock, G. J. (1992) Plate Slenderness Limits for High Strength Steel
728 Sections. Journal of Constructional Steel Research. 23, 73-96.
729 Pham, C.H. & Hancock, G. J. (2013) Experimental investigation and direct strength design of high-
730 strength, complex C-sections in pure bending. Journal of Structural Engineering. 139 (11), 1842-
731 1852.
732 Shi, G., Zhou, W.J., Bai, Y., Lin, C.C. (2014) Local buckling of 460 MPa high strength steel welded
733 section stub columns under axial compression. Journal of Constructional Steel Research. 100, 60-70.
734 Shi, G., Zhou, W.J., Lin, C.C. (2015) Experimental Investigation on the Local Buckling Behaviour of
735 960 MPa High Strength Steel Welded Section Stub Columns. Advances in Structural

736 Engineering.18(3), 423-438.
737 Shi, G., Xu, K.L., Ban, H.Y., & Lin, C. C. (2016). Local buckling behaviour of welded stub columns
738 with normal and high strength steels. Journal of Constructional Steel Research. 119, 144-153.
739 Shifferaw,Y. & Schafer, B. W. (2012) Inelastic Bending Capacity of Cold-Formed Steel Members.
740 Journal of Structural Engineering. 138(4), 468-480.
741 Standards Association of Australia (2016) AS 4100–1998: Reconfirmed 2016, Steel Structures.
742 Australian Standard, Committee BD-001, Sydney.
743 Standards Association of Australia (2020) AS 4100–2020: Reconfirmed 2016, Steel Structures.
744 Australian Standard, Sydney.
745 Su, A.D., Sun, Y., Liang, Y.T., Zhao, O. (2021) Membrane residual stresses and local buckling of
746 S960 ultra-high strength steel welded I-section stub columns. Thin-Walled Structures.161, 107497.
747 Sun, Y., Liang, Y.T., Zhao, O. (2019) Testing, numerical modelling and design of S690 high strength
748 steel welded I-section stub columns. Journal of Constructional Steel Research. 159, 521–533.
749 Timoshenko, S.P. & Gere, J.M. (1961) Theory of elastic stability. 2nd ed., New York, NY: McGraw-
750 Hill.
751 Tse, K., Wang, J., Yun, X. (2021) Structural behaviour and continuous strength method design of
752 high strength steel non-slender welded I-section beam–columns. Thin-Walled Structures. 169,
753 108273.
754 Yun, X., Zhu, Y.F., Gardner, L. (2021) Tests on high strength steel beams, columns and frames.
755 STROnger Steels in the Built Environment (STROBE), Work package Name and No: WP2- Plastic
756 Design with HSS, Deliverable: D2.2, London, UK.
757 Yun, X., Zhu, Y.F., Meng, X., Gardner, L. (2023) Welded steel I-section columns: Residual stresses,
758 testing, simulation and design. Engineering Structures. 282, 115631.
759 Yun, X. & Gardner, L. (2017) Stress–strain curves for hot-rolled steels. Journal of Constructional
760 Steel Research. 133, 36–46.
761 Zhao, O., Afshan, S., Gardner, L. (2017) Structural response and continuous strength method design
762 of slender stainless steel cross-sections. Engineering Structures. 140, 14-25.
763 Zhu, Y.F., Yun, X., Gardner, L. (2023) Numerical modelling and design of normal and high strength
764 steel non-slender welded I-section beam–columns. Thin-Walled Structures. 186, 110654.